# Damage Tolerance Analysis using the eXtended Finite Element Method

Mahmoud Rababah

A Thesis

in

The Department

of

Mechanical and Industrial Engineering

Presented in Partial Fulfillment of the Requirements

for the Degree of Master of Applied Science at

Concordia University

Montreal, Quebec, Canada

August, 2007

*Your file Votre référence*
*ISBN: 978-0-494-34643-3*
*Our file Notre référence*
*ISBN: 978-0-494-34643-3*

# ABSTRACT

Damage Tolerance Analysis using the eXtended Finite Element Method

Mahmoud Rababah

While the regular Finite Element Method (FEM) is well developed and robust, it is not particularly well suited to model evolving discontinuities, since the construction of a discontinuous space requires the element topology to be aligned with the geometry of the discontinuity. This in turn requires regeneration of the mesh as the discontinuity evolves, resulting in projection errors and a significant computational cost.

The eXtended Finite Element Method (XFEM) is a new technique which was developed recently to account for the evolving discontinuities in the crack growth problems. In XFEM, special functions (discontinuous and near tip functions) are added to the regular FEM to model the discontinuities without regenerating the mesh. Using this property in XFEM, and assuming Linear Elastic Fracture Mechanics (LEFM) concept, the damage tolerance analysis to determine the time or the number of loading cycles required for a smaller pre-existent crack to grow to critical size can be accomplished more efficiently than that in the regular FEM.

The derived XFEM-formulation has been effectively implemented and in-house computer code has been developed to find the stress intensity factors and to model the crack growth efficiently without re-meshing the structure. Numerous benchmark 2-D problems with cracks located at different locations and inclined in different angles have been investigated and the results are validated with those available in the literature.

Finally, the potential application of XFEM in damage tolerance analysis has been demonstrated.

# ACKNOWLEDGEMENTS

It is really an honour and a privilege to express my gratitude and indebtedness to my supervisor, Ramin Sedaghati for his priceless support, encouragement and inspiration. His wealth of knowledge, his critical and creative thinking has given me direction and insight in pursuing this research.

I treasure the invaluable support and encouragement of my parents. I also owe my loving thanks to my wife Nisreen Awwad. She has endured a lot from my research and traveling. Without her support, understanding and encouragement it would not be possible to complete this research.

Finally, I would like to personally thank all of my colleagues and friends who have been so supportive and giving of their time.

# DEDICATION

*for my parents, my wife and my son*

# TABLE OF CONTENTS

# LIST OF FIGURES

# LIST OF TABLES

# CHAPTER ONE

# INTRODUCTION

## 1.1 Motivations

High deformation, instability and fracture are examples of structural failure mechanisms. Fracture is a potentially catastrophic failure mechanism, characterized by un-stable and extremely fast crack growth. The starting point is often a small flaw in a region of stress concentration, which may develop into a crack. If the structure is submitted to cyclic loads then the crack grows, initially at very low rates, in a process known as fatigue crack growth. Stable and slow fatigue crack growth will take place until the crack reaches a critical length. At this moment, the structure is no longer capable of withstanding the service loads and fracture occurs.

In the late 1960s and for few years later, a number of aircraft structural failures occurred both during testing and in-service. Some of these failures were attributed to flaws or defects that were either inherent or introduced during the manufacturing and assembly of the structure. The presence of these flaws was not accounted for in design. The design was based on a "safe-life" fatigue analysis, where the mean life predictions were based upon fatigue test data and a conventional fatigue analysis for materials with no flaws or pre-existent cracks.

In order to ensure the safety of the aircraft structure the damage tolerance design was adopted in 1970s to replace the conventional fatigue design approach, and later many industrial fields adopted the damage tolerance analysis that shift the design concept from the crack initiation life to the crack propagation life. This approach is based on setting

inspection intervals required for a crack to grow from a detectable size to a critical size. These intervals are determined from the knowledge of the number of loading cycles

Although Finite Element Method (FEM) can be used to perform numerical crack growth analysis based on Linear Elastic Fracture Mechanics (LEFM) concepts, the design must start with the creation of complex discretized model representing the structure and great care should be considered when creating such a model. Due to the presence of the cracks, the model contains stress singularities at the crack tips and therefore the discretization around the crack tips has to be fine, usually requiring a large number of elements. Moreover, in a crack propagation analysis, it is generally necessary to re-mesh large portions of the problem domain in order to accommodate the changes to the position of the crack tips.

The boundary Element Method (BEM) has been introduced to fracture mechanics problems since the early 1970s. The main difference between the BEM and the FEM is that in the BEM, an analytical approach towards the solution is taken by the adoption of the fundamental solutions which satisfy the governing equation. In most cases a formulation is obtained which does not contain integrals over the problem domain, and consequently, does not require domain discretization. Therefore, only the boundary of the problem needs to be discretized into elements. But a fine discretization is still required near singularities. The BEM simplify the discretization requirements in the problem by incorporating into its formulation some knowledge about the solution of the governing equation in the form of fundamental solutions. As a consequent, the technique can only be applied for governing equations for which fundamental solutions are available.

Since FEM and BEM are not well suited to account for evolving discontinuities, the need arose to develop new techniques that require no re-meshing when the discontinuities evolve. As a result for these needs, several new techniques have been developed in the last few years to model cracks and crack growth without re-meshing.

## 1.2 Literature Review

The element-free Galerkin (EFG) method [1] is a recently developed method for fracture and crack growth. The interpolant in this method is described in terms of a set of nodes and surfaces of the model. This class of methods is often called meshless methods. The advantage of meshless methods is that it is possible to model arbitrary growth of cracks without re-meshing and adaptive refinement at the crack tip is easily accomplished. However, it is awkward and expensive to refine the array of nodes around a crack tip adequately to obtain sufficient accuracy.

Belytschko and Black [2] introduced new method to model cracks and crack growth by finite element with minimal re-meshing. By this method a crack arbitrarily aligned within the mesh can be represented by means of enrichment functions. The essential idea in this method is to add tip enrichment functions to the approximation which contains a discontinuous displacement field. The same span of functions developed by Fleming et al. [3] for the enrichment of the element-free Galerkin method is used. The method exploits the partition of unity property of finite elements which was noted by Melenk and Babuska [4, 5], namely that the some of the shape functions must be unity.

Since the crack tip enrichment functions alone are not readily applicable to long cracks or three dimensions, an improvement by Moes et al. [6] has been done by incorporating a discontinuous field across the crack faces away from the crack tip. As a

result, this enrichment method, also called eXtended Finite Element Method (XFEM), combines both the discontinuous enrichment function and the near-tip enrichment functions to the approximation of the finite element.

Modeling quasi-static crack growth in 2-D problems for isotropic and bimaterial media using XFEM is described in Sukumar and Prevost [7] in which the implementation of the crack growth using the XFEM within a general purpose finite element code is also described. The numerical applications are performed in Sukumar et al. [8].

New enrichment schemes are introduced in Bechet et al. [9] by proposing a geometrical enrichment which bears the characteristic of a constant enriched area within a prescribed geometry. These enrichment schemes allow more layers of elements to bear the complete enrichment basis (i.e. the size of enrichment area is no longer proportional to the element edge length and the accuracy is independent on the position of the crack tip).

In the particular case where the extent of the crack approaches the support size of the nodal shape functions, the asymptotic near tip functions for each tip may extend beyond the length of the crack, resulting in a non-conforming approximation. This particular case was solved in Bellec and Dolbow [10] by proposing a set of adjustments and modifications for the near-tip asymptotic functions.

A 2-D numerical model of micro structural effects and quasi-static crack propagation in brittle materials using XFEM is presented in Sukumar et al. [11]. Modeling of cracks with multiple branches, multiple holes and cracks emanating from holes are presented in Daux et al. [12]. The implementation is based on using the same enrichment functions for the cracks (discontinuous and tip functions) and the enrichment scheme is developed

based on the interaction of the discontinuous geometric features with the mesh. Whereas for holes, new enrichment function is introduced.

Modeling 3-D planar cracks by XFEM was first introduced in Sukumar et al. [13], who solved several planar crack mode-*I* problems and showed that the method compared well with analytical solutions. Moes et al [14] extended the methodology to handle arbitrary cracks in three dimensions. This was performed by describing the crack geometry in terms of two signed distance functions. The 3-D crack propagation was simulated in Sukumar et al. [15].

At this point, it should be emphasized that XFEM is still in its early stages, and more investigations are needed to use this promising technique in different fields; as it is still limited to model cracks and crack growth in structural geometries.

## 1.3 Objectives of the Study

The primary objective of this study is to validate the eXtended Finite Element Method for two dimensional problems containing cracks located at different locations and inclined in different angles and study the effect of the mesh type (quadrilateral and triangular), the mesh refinement and the radius of enrichment on the output results.

The second objective is to model the crack growth using the XFEM for edge and central cracks, and to predict the life time of structure with pre-existent crack to reach critical length using the damage tolerance analysis.

## 1.4 Organization of the Thesis

Chapter two provides brief review about the fracture mechanics; the concept of Linear Elastic Fracture Mechanics (LEFM) and when it can be adopted; the near tip

asymptotic fields; the loading modes and their interactions; the stress intensity factor and its relation with the plane stresses; fatigue and the crack growth and its direction.

Chapter three provides detailed description on how to perform the XFEM analysis and the difference between XFEM and the regular FEM; what nodes should be selected for the enrichment and how the enrichment will be performed; how to find the stiffnesses for the elements especially the elements that cut by the crack.

Chapter four provides full implementation details for the XFEM from programming point of view and how to find the first and second modes of the stress intensity factor with detailed description on how to implement this task. It also discusses some problems for cracks located at different locations and inclined with different angles and gives the full comparison between the results from the XFEM and the exact solutions.

Chapter five starts with defining the safe-life design and the damage tolerance design and explains the two approaches used in damage tolerance design with considering some catastrophic accidents happened in the past. It also discusses some studies for crack growth starting from pre-existence crack length to critical crack length. Prediction of the crack path and the life time before the crack grows to critical length is also investigated.

Finally chapter six summarized the work and provides some recommendations for the future work

# CHAPTER 2

# FRACTURE MECHANICS

## 2.1 Introduction

This chapter discusses some of the fundamental concepts in the fracture mechanics starting from the concept of the Linear Elastic Fracture Mechanics (LEFM) and its limitations, and then presents the asymptotic crack tip fields in LEFM for two dimensional structures. The concepts of fatigue and crack growth are also discussed. Finally the failure criterion for the mixed-mode problems is derived.

## 2.2 Linear Elastic Fracture Mechanics (LEFM) and its Limitations

The Linear Elastic Fracture Mechanics theory is based on the principles of the linear elastic theory, in which the bulk of the material behaves according to hook's law. If the zone of yielding around the crack tip is small compared to the dimensions of the problem (small scale yielding) then LEFM theory is applicable. Thus small scale yielding can be considered as a criterion for the LEFM and can be represented as the radius of the plastic zone circle $r_p$ a head of the crack tips as shown in Figure 2.1. For the structure loaded by pure mode-*I* with initial crack length $a$, the radius of the plastic zone can be described as [16]:

$$r_p = \frac{1}{2\pi}\left(\frac{K_I}{\sigma_{YS}}\right)^2 \qquad (2.1)$$

where $\sigma_{YS}$ is the Yield stress and $K_I$ is the stress intensity factor associated with mode-*I*. Now if $a >> r_p$, it can be considered that LEFM theory is applicable. Practically $a > 10r_p$ would be a good criterion for the application of LEFM.

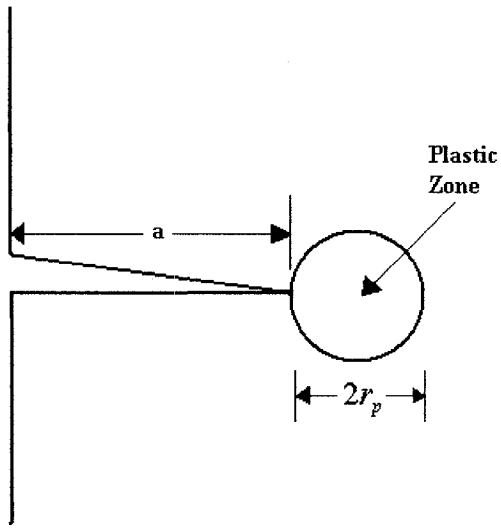


Figure 2.1: Crack tip plastic zone

It should be noted that for most industrial applications, neglecting plastic work is conservative since the development of plasticity in the crack tip region consumes energy that would, in an elastic material, be available to contribute to the crack advance. Thus, through all problems in this thesis, to be more conservative for the life time estimation of the crack propagation, the LEFM concept is assumed.

## 2.3 Numerical Fracture Mechanics

Numerical fracture mechanics is widely used in welded structures, pressure vessels, aircraft fuselage, bridges, ships and more other applications in which the fracture of the component in the system may lead to catastrophic results. The most concern issue when

studying these structures is the life time prediction that helps in preventing the catastrophic failure before it occurs. When the analytical methods fail to produce closed-form solutions for complex structures or flaws with complex geometries, the numerical methods become necessary, and obtaining the fracture parameters such as the Stress Intensity Factors (SIFs) numerically will be unavoidable. However still obtaining such fracture parameter remains a challenging problem.

The difficulties encountered when simulating crack growth is linked to the fact that computing the state of stress in a cracked body necessitates dealing with the discontinuities in some of the mechanical fields created by the cracks. In the regular FEM, this difficulty is solved making the elements edges aligned with the crack faces. However, this requires a costly mesh generation and regeneration, making the regular FEM cumbersome, especially for complex three-dimensional problems encountered in industry. One more difficulty is the singularity nature of the asymptotic crack tip fields that requires high mesh density in the tip region. Due to these difficulties, it is computationally very expensive to find the fracture parameters.

The boundary Element Method (BEM) has been applied to fracture mechanics problems since the early 1970s. The main difference between the BEM and the FEM is that in the BEM, an analytical approach towards the solution is taken by adopting the fundamental solutions which satisfy the governing equations. In most cases a formulation is obtained which does not contain integrals over the problem domain, and consequently, does not require domain discretization. Therefore, only the boundary of the problem needs to be discretized into elements, but, a fine discretization is still required near singularities.

From the preceding discussion, it is basically known that the BEM simplify the discretization requirements in the problem by incorporating into its formulation some knowledge about the solution of the governing equation in the form of fundamental solutions. The technique can only be applied for governing equations for which fundamental solutions are available.

Cruse [17] showed that existence of coinciding boundary nodes in opposite crack surfaces causes singular matrix in direct application of the BEM. This is because the nodes have the same coordinates, and the integrals are calculated along the same paths. In order to avoid modeling the crack, Synder and Cruse [18] proposed the use of a special fundamental solution, known as the crack green's function, which identically satisfies the boundary conditions for a traction free crack in an infinite plate. Although the technique is accurate, it is limited to two dimensional straight cracks. For more literature regarding developments of the BEM and its use in some structural problems it can be referred to Salgado [19].

The eXtended Finite Element Method (XFEM) has recently considered as a powerful alternative numerical approach in fracture mechanics, it overcomes the two shortcomings associated with discontinuity of the displacement field across the crack faces and with singularity of the stress field at the crack tip. Also, the close similarity between XFEM and the regular FEM allow the easiness of merging the XFEM with the commercial finite element packages.

## 2.4 Crack Tip Asymptotic Fields in LEFM

The crack is defined as line of discontinuity in two dimensions and surface of discontinuity in three dimensions. The crack could be loaded in three different ways as shown in Figure 2.2 known as opening, shearing and tearing modes.

Generally, the crack tip stress, strain and displacement fields may be represented as a linear combination of these modes.

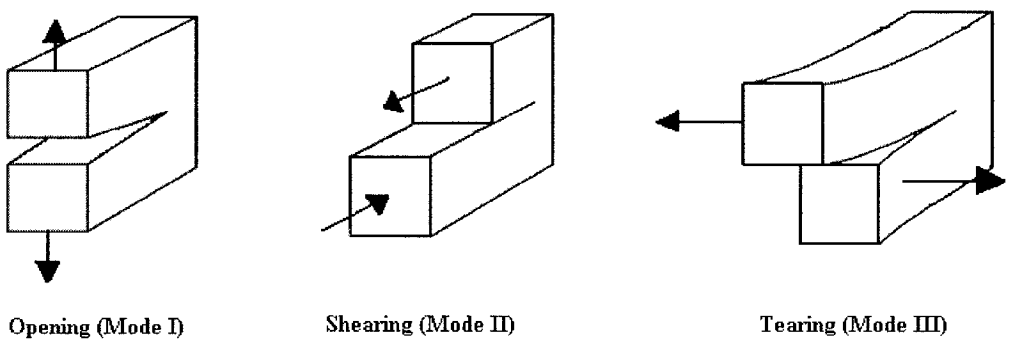


Figure 2.2: Modes of crack tip deformation

Each deformation mode shown above can be expressed in terms of stress developed at the crack tip asymptotic field using suitable functions. Moreover, for each mode, the magnitude of the stress field is defined by a scalar coefficient called the Stress Intensity Factor (SIF). There is only one stress intensity factor for each loading mode that will be referred to as $K_I$ for the opening mode, $K_{II}$ for the shearing mode and $K_{III}$ for the tearing mode. A crack is said to be loaded in mixed-mode when more than one stress intensity factor is necessary to represent the crack tip asymptotic fields.

During this work, only two dimensional problems are considered; so the tearing mode is not accounted for in this work and only the first two modes of the Stress Intensity Factor (SIF) are considered. The crack tip asymptotic field for mode-*I* and mode-*II* can be written as [20]:

Mode *I*:

$$\begin{Bmatrix}\sigma_{xx}\\ \sigma_{yy}\\ \tau_{xy}\end{Bmatrix}=\frac{K_I}{\sqrt{2\pi r}}\begin{Bmatrix}\cos\frac{\theta}{2}(1-\sin\frac{\theta}{2}\sin\frac{3\theta}{2})\\ \cos\frac{\theta}{2}(1+\sin\frac{\theta}{2}\sin\frac{3\theta}{2})\\ \cos\frac{\theta}{2}\sin\frac{\theta}{2}\cos\frac{3\theta}{2}\end{Bmatrix} \tag{2.2}$$

$$\begin{Bmatrix}u_x\\ u_y\end{Bmatrix}=\frac{K_I}{2\mu}\sqrt{\frac{r}{2\pi}}\begin{Bmatrix}\cos\frac{\theta}{2}\left[\kappa-1+2\sin^2\frac{\theta}{2}\right]\\ \sin\frac{\theta}{2}\left[\kappa+1-2\cos^2\frac{\theta}{2}\right]\end{Bmatrix} \tag{2.3}$$

where $K_I$ is the mode-*I* stress intensity factor defined as

$$K_I=\sqrt{2\pi r}\lim_{r\to 0}\sigma_{yy}(r,0) \tag{2.4}$$

Mode-*II*:

$$\begin{Bmatrix}\sigma_{xx}\\ \sigma_{yy}\\ \tau_{xy}\end{Bmatrix}=\frac{K_{II}}{\sqrt{2\pi r}}\begin{Bmatrix}-\sin\frac{\theta}{2}(2+\cos\frac{\theta}{2}\cos\frac{3\theta}{2})\\ \sin\frac{\theta}{2}\cos\frac{\theta}{2}\cos\frac{3\theta}{2}\\ \cos\frac{\theta}{2}(1-\sin\frac{\theta}{2}\sin\frac{3\theta}{2})\end{Bmatrix} \tag{2.5}$$

$$\begin{Bmatrix}u_x\\ u_y\end{Bmatrix}=\frac{K_{II}}{2\mu}\sqrt{\frac{r}{2\pi}}\begin{Bmatrix}\sin\frac{\theta}{2}\left[\kappa+1+2\cos^2\frac{\theta}{2}\right]\\ -\cos\frac{\theta}{2}\left[\kappa-1-2\sin^2\frac{\theta}{2}\right]\end{Bmatrix} \tag{2.6}$$

where $K_{II}$ is the mode-*II* stress intensity factor defined as

$$K_{II} = \sqrt{2\pi r} \lim_{r \to 0} \tau_{xy}(r, 0) \tag{2.7}$$

Where $\mu$ is the shear modulus and $\kappa = (3-\upsilon)/(1+\upsilon)$ for the plane stress condition and $\kappa = 3-4\upsilon$ for the plane strain condition. $r, \theta$ are the local polar coordinates at the crack tips as shown in Figure 2.3.

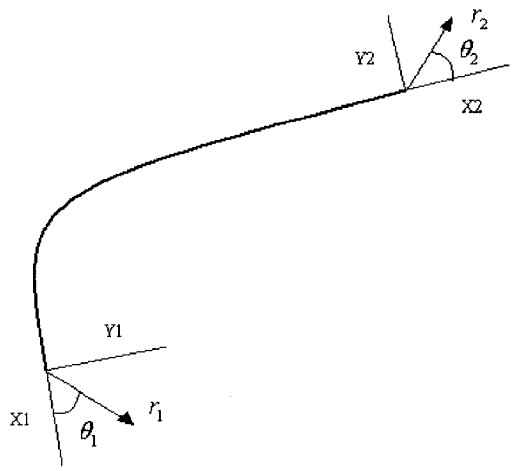


Figure 2.3: Crack local coordinates at the crack tips

In 2-D mixed-mode loading, mode-*I* and mode-*II* are necessary to represent the crack tip asymptotic fields which can be written as [20]:

$$\begin{Bmatrix} \sigma_{xx} \\ \sigma_{yy} \\ \tau_{xy} \end{Bmatrix} = \frac{K_I}{\sqrt{2\pi r}} \begin{Bmatrix} \cos\frac{\theta}{2}(1-\sin\frac{\theta}{2}\sin\frac{3\theta}{2}) \\ \cos\frac{\theta}{2}(1+\sin\frac{\theta}{2}\sin\frac{3\theta}{2}) \\ \cos\frac{\theta}{2}\sin\frac{\theta}{2}\cos\frac{3\theta}{2} \end{Bmatrix} + \frac{K_{II}}{\sqrt{2\pi r}} \begin{Bmatrix} -\sin\frac{\theta}{2}(2+\cos\frac{\theta}{2}\cos\frac{3\theta}{2}) \\ \sin\frac{\theta}{2}\cos\frac{\theta}{2}\cos\frac{3\theta}{2} \\ \cos\frac{\theta}{2}(1-\sin\frac{\theta}{2}\sin\frac{3\theta}{2}) \end{Bmatrix} \tag{2.8}$$

$$\begin{Bmatrix} u_x \\ u_y \end{Bmatrix} = \frac{K_I}{2\mu}\sqrt{\frac{r}{2\pi}} \begin{Bmatrix} \cos\frac{\theta}{2}\left[\kappa - 1 + 2\sin^2\frac{\theta}{2}\right] \\ \sin\frac{\theta}{2}\left[\kappa + 1 - 2\cos^2\frac{\theta}{2}\right] \end{Bmatrix} + \frac{K_{II}}{2\mu}\sqrt{\frac{r}{2\pi}} \begin{Bmatrix} \sin\frac{\theta}{2}\left[\kappa + 1 + 2\cos^2\frac{\theta}{2}\right] \\ -\cos\frac{\theta}{2}\left[\kappa - 1 - 2\sin^2\frac{\theta}{2}\right] \end{Bmatrix} \tag{2.9}$$

## 2.5 Fatigue

Relating the crack growth to the LEFM parameters such as the stress intensity factor makes it possible to predict the crack growth rate under cyclic loading. Thus the structure life time or the number of cyclic loading required for a crack to grow from its initial length up to the critical length causing catastrophic failure can be determined. Paris and Paris [21] proposed a law for fatigue crack growth relating the increment in crack advance $da$ to the increment in number of cycles $dN$ and the stress intensity factor range $\Delta K$ as:

$$\frac{da}{dN} = C_p(\Delta K)^{m_p} \tag{2.10}$$

Where $C_p$ and $m_p$ are material constants, determined experimentally by standard fatigue tests and $\Delta K = K_{\max} - K_{\min}$ is the stress intensity factor range.

In literature, different fatigue crack growth equations have been developed based on the curve fitting techniques using computer programs. Two of these equations are provided below [22, 23]:

Forman Equation:

$$\frac{da}{dN} = \frac{C_p(\Delta K)^{m_p}}{(1-R)K_c - \Delta K} \tag{2.11}$$

Walker Equation:

$$\frac{da}{dN} = C_p \left[ K_{\max} (1-R)^{m_p} \right]^{n_p} \tag{2.12}$$

where $R$ is the stress ratio defined as $R = \frac{\sigma_{\min}}{\sigma_{\max}}$

There are three stages characterizing fatigue crack growth as shown in Figure 2.4. Stage-*I* begins with a threshold value of stress intensity factor, $\Delta K_{threshold}$. Before this stage no crack propagation occurs. This stage continues until the curve becomes linear.

Stage-*II* represents the zone in which the relationship between $\ln \frac{da}{dN}$ and $\ln \Delta K$ is linear. In this stage, fatigue crack growth is governed by the Paris law. The life of many cracked engineering structures may be considered solely in this range since the allowances are made for the minimum crack length that can be inspected, which is normally related to the limitations of the inspection techniques used. For instance, the parameter that is controllable in practical situations is the inspection interval (i.e. the time interval between two successive nondestructive evaluations of the structure of interest).

Stage-*III* exhibits a sharp slope, where a small increment in the stress intensity factor range $\Delta K$ leads to a large increment in crack advance per cycle $\frac{da}{dN}$. The material behavior in this stage is complicated where the plastic zone becomes to be large compared to the structural geometry.

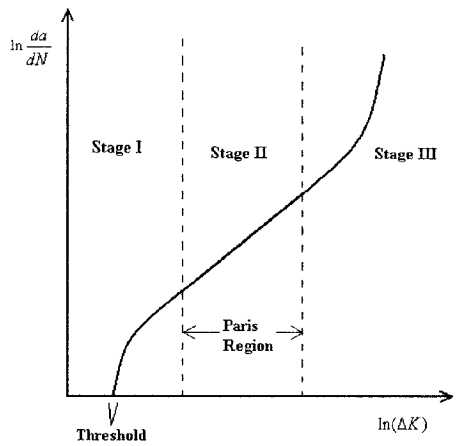


Figure 2.4: Fatigue crack stages

For mixed-mode problems, the stress intensity factor $\Delta K$ can be replaced by equivalent one, $\Delta K_e$, which can be described as [24]:

$$\Delta K_e = \sqrt{\Delta K_I^2 + 2\Delta K_{II}^2} \tag{2.13}$$

## 2.6 Crack Growth

The crack growth considered in this work is quasi-static crack growth, where the inertia effects are neglected. Modeling crack growth requires (besides knowing the increment of the crack) knowing the direction, in which the crack will extend. Many criteria have been used to determine the crack growth direction such as the maximum energy release rate criterion [25], the minimum strain energy density criterion [26] and the maximum principal stress criterion [27].

Since the maximum principle stress criterion is one of the most commonly used, it is adopted during all the crack growth analysis done in this thesis. It states that the crack will propagate from its tip in a direction $\theta = \theta_c$, such that the circumferential stress $\sigma_{\theta\theta}$ is maximum. The usual polar coordinate system related to the crack tip is used to describe

the crack propagation direction. Since $\sigma_{\theta\theta}$ is principal stress in the direction of crack propagation, the crack will propagate in the direction such that the shear stress is zero. Setting the shear stress to zero in the expression for the asymptotic crack tip fields of LEFM allows the determination of the value of the crack propagation angle. The derivation is performed as follow:

First, the stress transformation is performed as shown in Figure 2.5 to transform the stresses from the Cartesian *xx-yy* coordinates to the polar coordinates *r-θ* as:

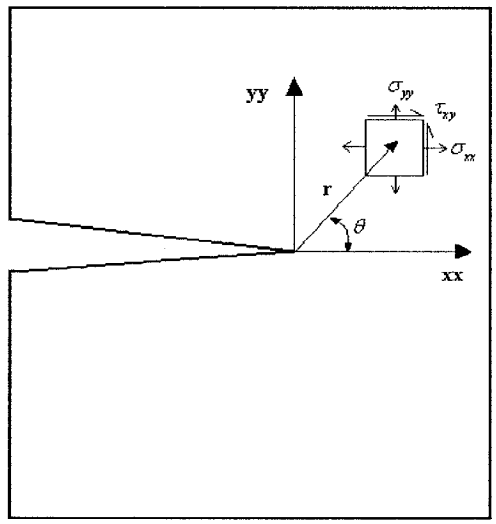


Figure 2.5: Near tip asymptotic field transformation

$$\begin{bmatrix} \sigma_{rr} & \tau_{r\theta} \\ \tau_{r\theta} & \sigma_{\theta\theta} \end{bmatrix} = T \begin{bmatrix} \sigma_{xx} & \tau_{xy} \\ \tau_{xy} & \sigma_{yy} \end{bmatrix} T^T \tag{2.14}$$

where $T$ is the transformation matrix defined as $T = \begin{bmatrix} \cos\theta & \sin\theta \\ -\sin\theta & \cos\theta \end{bmatrix}$ and $\sigma_{xx}, \sigma_{yy}$ and $\tau_{xy}$ are obtained from Eq. (2.8). Now using Eq. (2.14), we can write:

$$\tau_{r\theta} = \frac{1}{\sqrt{2\pi r}} \cos\frac{\theta}{2}\left[\frac{1}{2}K_I \sin\theta + \frac{1}{2}K_{II}(3\cos\theta - 1)\right] \qquad (2.15)$$

The crack will grow in direction where the shear $\tau_{r\theta}$ is zero. Thus setting $\tau_{r\theta} = 0$ yields:

$$K_I \sin\theta_c + K_{II}(3\cos\theta_c - 1) = 0 \qquad (2.16)$$

Solving this equation for $\theta_c$ gives:

$$\theta_c = 2\tan^{-1}\frac{1}{4}\left(\frac{K_I}{K_{II}} \pm \sqrt{\left(\frac{K_I}{K_{II}}\right)^2 + 8}\right) \qquad (2.17)$$

The sign $(\pm)$ in Eq. (2.17) can be chosen based on the fact that if $K_{II} = 0$ then $\theta_c = 0$ (pure mode-*I*) and if $K_{II} > 0$, then $\theta_c < 0$, and if $K_{II} < 0$, then $\theta_c > 0$ .

## 2.7 Fracture Failure Criteria

In pure mode-*I* loading, the fracture occurs when the stress intensity factor $K_I$ developed in the crack tip field reaches critical value $K_{IC}$ called the fracture toughness. The fracture toughness is a material property obtained experimentally. The principal stress at fracture, $\sigma_1^I$, can be obtained from Eq. (2.2) by replacing $K_I$ by $K_{IC}$ and setting $\theta = 0$:

$$\sigma_1^I = \frac{K_{IC}}{\sqrt{2\pi r}} \qquad (2.18)$$

In mixed-mode fracture, assuming that the crack growth occurs according to the maximum principle stress criterion, then $\sigma_{\theta\theta}$ can be obtained from Eq. (2.14) as:

$$\sigma_{\theta\theta} = \frac{1}{\sqrt{2\pi r}} \cos^2\frac{\theta}{2}\left[K_I \cos\frac{\theta}{2} - 3K_{II}\sin\frac{\theta}{2}\right] \qquad (2.19)$$

then the value of the maximum principal stress can be obtained by replacing $\theta$ with $\theta_c$ :

$$\sigma_1 = \frac{1}{\sqrt{2\pi r}} \cos^2 \frac{\theta_c}{2} \left[ K_I \cos \frac{\theta_c}{2} - 3K_{II} \sin \frac{\theta_c}{2} \right] \tag{2.20}$$

It is postulated that in mixed-mode, fracture takes place when the maximum principal stress $\sigma_1$ reaches $\sigma_1^I$ in pure mode-*I*. Equating Eqs. (2.18) and (2.20), one may obtain:

$$K_{IC} = \cos^2 \frac{\theta_c}{2} \left[ K_I \cos \frac{\theta_c}{2} - 3K_{II} \sin \frac{\theta_c}{2} \right] \tag{2.21}$$

The term in the right hand side of Eq. (2.21) is refereed to $K_{Ieq}$. Thus in summary, the fracture in mixed-mode condition occurs when:

$$K_{Ieq} \geq K_{IC} \tag{2.22}$$

where

$$K_{Ieq} = \cos^2 \frac{\theta_c}{2} \left[ K_I \cos \frac{\theta_c}{2} - 3K_{II} \sin \frac{\theta_c}{2} \right] \tag{2.23}$$

## 2.8 Conclusion

The regular FEM is not well-suited for geometries with evolving discontinuities as it requires re-meshing as the discontinuity evolves. Also, it requires high mesh density in the crack tip region due to the singularities which cause high computational cost.

On the other hand, BEM requires some knowledge about the solution of the governing equation in the form of fundamental solution. Thus, the technique can only be applied for governing equations for which fundamental solutions are available and it fails for three dimensional complicated geometries with kink cracks. The XFEM is well-suited for such problems that contain evolving discontinuities as there is no need for re-meshing the domain as the discontinuities evolve.

The LEFM can be employed to evaluate the stress intensity factor as it provides non-coasting time results. Also Paris law can be effectively used to determine the life time of a specimen by calculating the number of cycles required for a crack to grow from its initial length to the critical length.

Finally the criteria for the crack growth directions and fracture failure for mixed-mode problems were established.

# CHAPTER THREE

# EXTENDED FINITE ELEMENT METHOD-FORMULATION

## 3.1 Introduction

This chapter discusses the XFEM technique used to model two dimensional mechanical structures with pre-existent cracks, where the cracks are located at different locations and inclined in different angles. First the XFEM approximation solution is derived followed by the enrichment scheme for the nodes in the background mesh. Modeling the cracks in 2-D domain, the procedure to obtain the element stiffness matrix and the extra degrees of freedom resulted from the nodes enrichment are fully described.

Two types of background mesh namely isoparametric quadrilateral element mesh and the constant-strain triangular element mesh are used to discretize the domain. Results obtained from XFEM for both types are compared with analytical results to validate the formulation.

## 3.2 Extended Finite Element Method

In the FEM the crack is modeled explicitly by conforming the crack faces to the elements edges. Thus, re-meshing the domain each time the crack grows is unavoidable. On the other side, in the XFEM the domain is first discretized, then the crack is modeled implicitly by enriching the nodes in the crack region by the enrichment functions. The nodes are enriched through enrichment scheme discussed in this section.

### 3.2.1 Crack modeling using XFEM

Before modeling the crack using XFEM, the domain should be discretized. This can be performed using the regular finite element discretization. Two types of discretization are considered in this study; the quadrilateral element mesh and the constant-strain triangular element mesh. However, it is possible to combine both types in one discretization model. Using higher order elements mesh with the XFEM is still in its early stages and no much work has been done in this trend.

The approximation solution containing the discontinuous enrichment function (also called Heaviside function) is first introduced by Moes et al. [6]. Moes introduced the notation of the Heaviside function enrichment by considering a simple case for crack aligned with the edges of the elements in the mesh and the crack tip exactly coincide with one of the nodes as shown in Figure 3.1. The finite element approximation for this case is:

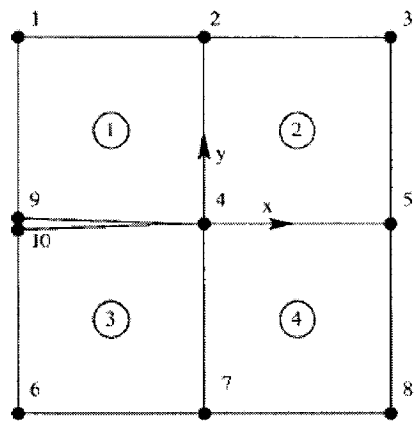


Figure 3.1: Heaviside elementary case [6]

$$u^h = \sum_{i=1}^{10} u_i \varphi_i \tag{3.1}$$

where $u_i$ is the displacement at node $i$ and $\varphi_i$ is the bilinear shape function associated with node $i$. Defining parameters $a$ and $b$ as:

$$a = \frac{u_9 + u_{10}}{2}, \quad b = \frac{u_9 - u_{10}}{2} \tag{3.2}$$

One can express $u_9$ and $u_{10}$ as:

$$u_9 = a + b, \quad u_{10} = a - b \tag{3.3}$$

Now substituting $u_9$ and $u_{10}$ into Eq. (3.1) yields

$$u^h = \sum_{i=1}^{8} u_i \varphi_i + a(\varphi_9 + \varphi_{10}) + b(\varphi_9 + \varphi_{10}) H(x) \tag{3.4}$$

Where *H(x)* is referred here as a discontinuous function (Heaviside function), and is defined in the local crack coordinate system as shown in Figure 3.1 as:

$$H(x, y) = \begin{cases} 1 & y > 0 \\ -1 & y < 0 \end{cases} \tag{3.5}$$

Considering this and referring to Figure 3.1 in which the crack is aligned with the element edge, *H(x)* is equal to 1 on element 1 and -1 on element 3. Eq. (3.4) can also be rewritten in the following form:

$$u^h = \sum_{i=1}^{8} u_i \varphi_i + u_{11} \varphi_{11} + b \varphi_{11} H(x) \tag{3.6}$$

where $\varphi_{11} = \varphi_9 + \varphi_{10}$ and $u_{11} = a$

The first two terms on the right-hand side of Eq. (3.6) represent the classical finite element approximation, whereas the last term represents the addition of a discontinuous enrichment.

In the case when the crack does not aligned with the element edges, the issue will be the selection of the appropriate nodes to be enriched, and the form of the associated enrichment function. It should be noted that in more general case where the crack is not aligned with the element edges and the crack tip does not coincide with the element edge, the discontinuity can not be described using only the Heaviside function.

For seamlessly modeling the entire discontinuity along the crack, the nodes belong to the element that contains the crack tip should be enriched by near-tip asymptotic functions. Considering this, the discretization approximation in XFEM can be described as [4]:

$$u^h = \sum_{i \in I} u_i \varphi_i + \sum_{j \in J} b_j \varphi_j H(x) + \sum_{k \in K_1} \varphi_k \left( \sum_{l=1}^{4} c_k^{l1} F_l^1(x) \right) + \sum_{k \in k_2} \varphi_k \left( \sum_{l=1}^{4} c_k^{l2} F_l^2(x) \right) \tag{3.7}$$

where

$$\{F_l(r,\theta)\} \equiv \left\{ \sqrt{r}\sin\left(\frac{\theta}{2}\right), \sqrt{r}\cos\left(\frac{\theta}{2}\right), \sqrt{r}\sin\left(\frac{\theta}{2}\right)\sin(\theta), \sqrt{r}\cos\left(\frac{\theta}{2}\right)\sin(\theta) \right\} \tag{3.8}$$

where $r$ and $\theta$ are the local polar coordinate at the crack tips; $I$ is the set contains all the nodes in the mesh; $J$ is the set that contains the nodes enriched by the discontinuity function (Heaviside function); $K_1$ and $K_2$ are the sets that contain the nodes enriched by the near-tip asymptotic functions for crack tip 1 and tip 2, respectively as shown in Figure 3.2.

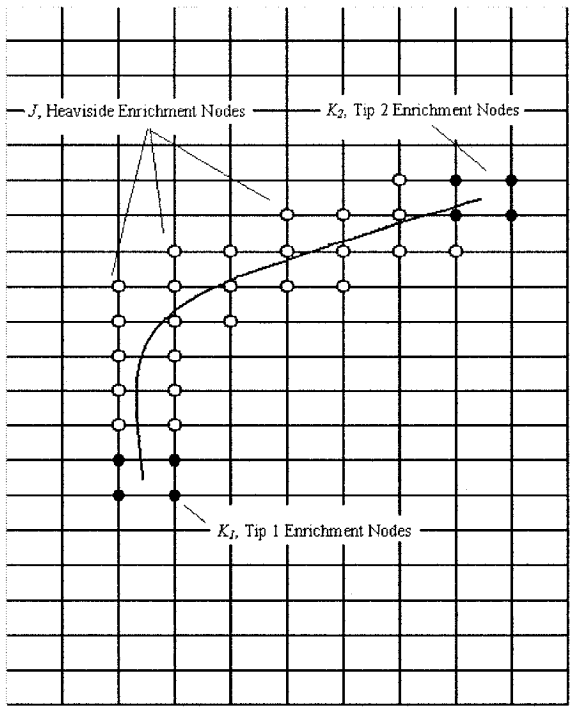


Figure 3.2: Nodal sets enrichment

This enrichment scheme mentioned above has the drawback that the accuracy depends on the position of the crack tip (for instance close to a node or an edge), and this is because there is only one layer of elements bears the complete enrichment basis, (i.e. the size of the enriched area is proportional to the element edge size $h_e$). An improvement on the enrichment scheme is studied by enriching not only the nodes that belong to the elements that contain the crack tip, but also all the nodes that located inside a geometrical area using the same enrichment functions [9]. Figure 3.3 shows that all nodes located inside the circle of enrichment that has the crack tip as its center will be enriched by the asymptotic near-tip functions. The radius of the circle can be selected based on the geometry of the sample and the crack.

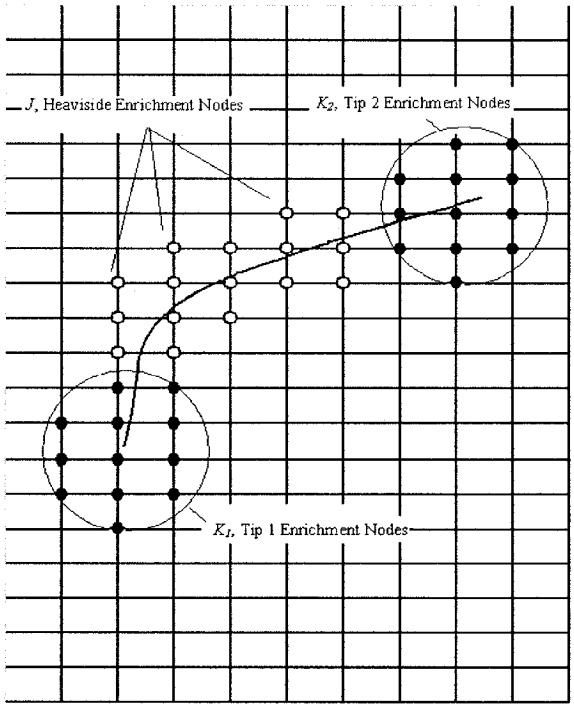


Figure 3.3: Modified nodal sets enrichment

### 3.2.2 Nodes enrichment scheme

The domain considered is two-dimensional domain. Extending the domain to three-dimensions is straight forward but it involves more implementation complications. Also in this work, the crack is considered as piecewise linear segments.

After establishing the background mesh (domain discretization) which can be performed using regular finite element mesh generator, each node is checked to see if its support area is cut by the crack. If it is cut, then the area criterion $\frac{A_w}{A} > 1\times10^{-4}$ will be checked. If this criterion is not satisfied, the node is excluded from the enrichment and treated as regular finite element node ($A_w$ is the smallest area resulted when the crack passes the support area of the node and $A$ is the total support area). If the area criterion is

satisfied, the node will be enriched by the discontinuity function. The support area $\omega_I$ of the node $I$ as shown in Figure 3.4 is defined as the area of all the elements that share that node.

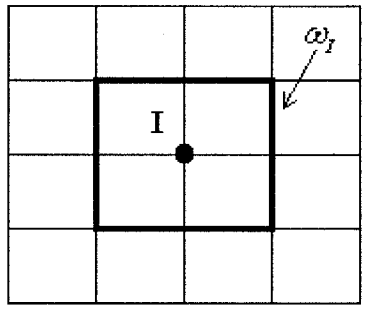


Figure 3.4 Support area $\omega_I$ for node I.

As mentioned before, the crack tip enrichment is performed based on geometrical enrichment scheme. The geometrical enrichment field is considered as circle centered at the crack tip with radius of enrichment $R_{enrich}$. If the node is located inside the circle, it will be enriched by the tip enrichment functions.

## 3.3 Element Stiffness Equation

Consider the 2-D domain $\Omega$ bounded by the boundary $\Gamma$ as shown in Figure 3.5 where the boundary $\Gamma$ is composed of $\Gamma_u$, $\Gamma_t$ and $\Gamma_c$. The prescribed displacements are imposed on the boundary $\Gamma_u$, the tractions are imposed on the boundary $\Gamma_t$ and the crack line $\Gamma_c$ is assumed to be traction-free.

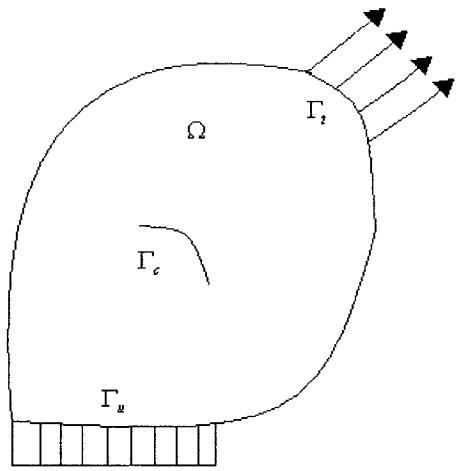


Figure 3.5: 2-D Domain boundaries

The equilibrium equations and the boundary conditions for linear elastic isotropic domain can be written as:

$$\nabla.\sigma + b = 0 \quad \text{in } \Omega \tag{3.9-a}$$

$$\sigma.n = \bar{t} \quad \text{on } \Gamma_t \tag{3.9-b}$$

$$\sigma.n = 0 \quad \text{on } \Gamma_{c^+} \tag{3.9-c}$$

$$\sigma.n = 0 \quad \text{on } \Gamma_{c^-} \tag{3.9-d}$$

$$u = \bar{u} \quad \text{on } \Gamma_u \tag{3.9-e}$$

where $n$ is the unit outward normal, $\sigma$ is the stress tensor and $b$ is the body force per unite volume. The strain-displacement relation can also be written as:

$$\varepsilon = \nabla_s u \tag{3.10}$$

where $\nabla_s$ is the symmetric part of the gradient operator. The stress-strain relation can be written as:

$$\sigma = C : \varepsilon \tag{3.11}$$

where $C$ is the Hooke tensor. By substituting the XFEM approximation in the linear elasto-static weak form [2], the discrete system of linear equations is obtained as:

$$[K]\{d\} = \{f^{ext}\} \tag{3.12}$$

where $d$ is the nodal displacement vector, $K$ is the global stiffness matrix and $f^{ext}$ is the external nodal force vector. The stiffness matrix and the force vector are computed on an element-by-element basis. Considering quadrilateral element, its contribution to $K$ and $f^{ext}$ can be written as:

$$k^e = \begin{bmatrix} [k^e_{11}] & [k^e_{12}] & [k^e_{13}] & [k^e_{14}] \\ [k^e_{21}] & [k^e_{22}] & [k^e_{23}] & [k^e_{24}] \\ [k^e_{31}] & [k^e_{32}] & [k^e_{33}] & [k^e_{34}] \\ [k^e_{41}] & [k^e_{42}] & [k^e_{43}] & [k^e_{43}] \end{bmatrix} \tag{3.13}$$

where each sub-matrix in Eq. (3.13) contains:

$$[k^e_{ij}] = \begin{bmatrix} [k^{uu}_{ij}] & [k^{ua}_{ij}] & [k^{ub}_{ij}] \\ [k^{au}_{ij}] & [k^{aa}_{ij}] & [k^{ab}_{ij}] \\ [k^{bu}_{ij}] & [k^{ba}_{ij}] & [k^{bb}_{ij}] \end{bmatrix} \tag{3.14}$$

where i, j = 1, 2, 3 for triangular elements and i, j = 1, 2, 3, 4 for quadrilateral elements, the $u$ represents the regular degrees, $a$ represents the discontinuity enrichment and $b$ represents the tip enrichments. The matrix in Eq. (3.14) can be obtained using the equation [4]:

$$[k^{rs}_{ij}] = \int_{\Omega^e} (B^r_i)^T C \; B^s_j d\Omega \qquad r,s = u,a,b \tag{3.15}$$

in which

$$B_i^u = \begin{bmatrix} \varphi_{i,x} & 0 \\ 0 & \varphi_{i,y} \\ \varphi_{i,y} & \varphi_{i,x} \end{bmatrix} \tag{3.16-a}$$

$$B_i^a = \begin{bmatrix} (\varphi_i H)_{,x} & 0 \\ 0 & (\varphi_i H)_{,y} \\ (\varphi_i H)_{,y} & (\varphi_i H)_{,x} \end{bmatrix} \tag{3.16-b}$$

$$B_i^b = \begin{bmatrix} (\varphi_i F_1)_{,x} & 0 & (\varphi_i F_2)_{,x} & 0 & (\varphi_i F_3)_{,x} & 0 & (\varphi_i F_4)_{,x} & 0 \\ 0 & (\varphi_i F_1)_{,y} & 0 & (\varphi_i F_2)_{,y} & 0 & (\varphi_i F_3)_{,y} & 0 & (\varphi_i F_4)_{,y} \\ (\varphi_i F_1)_{,y} & (\varphi_i F_1)_{,x} & (\varphi_i F_2)_{,y} & (\varphi_i F_2)_{,x} & (\varphi_i F_3)_{,y} & (\varphi_i F_3)_{,x} & (\varphi_i F_4)_{,y} & (\varphi_i F_4)_{,x} \end{bmatrix} \tag{3.16-c}$$

and

$$F_1 = \sqrt{r}\sin\left(\frac{\theta}{2}\right),\ F_2 = \sqrt{r}\cos\left(\frac{\theta}{2}\right),\ F_3 = \sqrt{r}\sin\left(\frac{\theta}{2}\right)\sin(\theta) \text{ and } F_4 = \sqrt{r}\cos\left(\frac{\theta}{2}\right)\sin(\theta) \tag{3.17}$$

It is noted from Eqs. (3.15) and (3.16) that $[k_{ij}^{uu}]$, $[k_{ij}^{ua}]$, $[k_{ij}^{au}]$ and $[k_{ij}^{aa}]$ are $2\times 2$ sub-matrices, $[k_{ij}^{ub}]$ and $[k_{ij}^{ab}]$ are $2\times 8$ , $[k_{ij}^{bu}]$ and $[k_{ij}^{ba}]$ are $8\times 2$ and $[k_{ij}^{bb}]$ is $8\times 8$ sub-matrix. Now if for instance the first node in the element is regular finite element node, then we have:

$$[k_{11}^e] = \begin{bmatrix} [k_{11}^{uu}] & [\ \ ] & [\ \ ] \\ [\ \ ] & [\ \ ] & [\ \ ] \\ [\ \ ] & [\ \ ] & [\ \ ] \end{bmatrix} \text{ or simply } [k_{11}^e] = [k_{11}^{uu}] \tag{3.18}$$

this is because $B^a$ and $B^b$ are empty matrices, also if the node is enriched by the discontinuity function, then $[k_{11}^e]$ can be written as:

$$[k_{11}^e] = \begin{bmatrix} [k_{11}^{uu}] & [k_{11}^{ua}] & [\ \ ] \\ [k_{11}^{au}] & [k_{11}^{aa}] & [\ \ ] \\ [\ \ ] & [\ \ ] & [\ \ ] \end{bmatrix} \tag{3.19}$$

where [ ] indicates an empty sub-matrix. And if the node is tip enrichment node, then $[k_{11}^{e}]$ can be written as:

$$[k_{11}^{e}]=\begin{bmatrix} [k_{11}^{uu}] & [\ ] & [k_{11}^{ub}] \\ [\ ] & [\ ] & [\ ] \\ [k_{11}^{bu}] & [\ ] & [k_{11}^{bb}] \end{bmatrix} \tag{3.20}$$

The element force vector for the quadrilateral element can be represented as:

$$\{f^{e}\}=\left\{\{f_1^{e}\} \quad \{f_2^{e}\} \quad \{f_3^{e}\} \quad \{f_4^{e}\}\right\}^{T} \tag{3.21}$$

each sub-vector $i$ in Eq. (3.21) is composed of [4]:

$$\{f_i^{e}\}=\left\{\{f_i^{u}\} \quad \{f_i^{a}\} \quad \{f_i^{b1}\} \quad \{f_i^{b2}\} \quad \{f_i^{b3}\} \quad \{f_i^{b4}\}\right\}^{T} \tag{3.21}$$

where

$$\begin{aligned} \{f_i^{u}\} &= \int_{\partial\Omega_t^h \cap \partial\Omega^e} \varphi_i \bar{t} d\Gamma + \int_{\Omega^e} \varphi_i b d\Omega \\ \{f_i^{a}\} &= \int_{\partial\Omega_t^h \cap \partial\Omega^e} \varphi_i H \bar{t} d\Gamma + \int_{\Omega^e} \varphi_i H b d\Omega \\ \{f_i^{b\alpha}\} &= \int_{\partial\Omega_t^h \cap \partial\Omega^e} \varphi_i F_l \bar{t} d\Gamma + \int_{\Omega^e} \varphi_i F_l b d\Omega \qquad \alpha = 1-4 \end{aligned} \tag{3.22}$$

it should be mentioned that for the traction-free crack $\{f_i^{a}\}$ and $\{f_i^{b}\}$ are empty vectors and $\{f_i^{e}\}=\{f_i^{u}\}$.

## 3.4 Types of Elements

Two types of domain discretization are considered using constant-strain triangular elements and isoparametric quadrilateral elements. In both types the same enrichment scheme is followed. This means that the node will be enriched if its support is cut by the crack or if it is located inside the geometrical enrichment field for tip 1 or tip 2 as shown

in Figure 3.6. The same distinctions for the nodes (regular or enriched by discontinuity function or tip enrichment functions) are applied. Moreover the same distinctions for the elements (regular elements, these containing extra degrees of freedom or these cut by the crack) are applied.

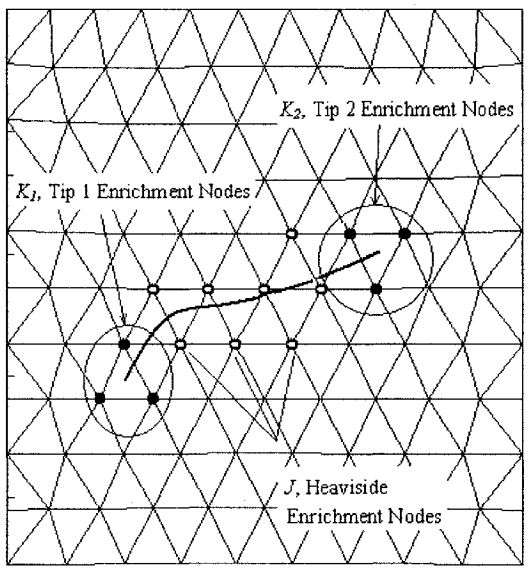


Figure 3.6: Enrichment nodes sets for constant-strain triangular mesh

The only difference between these discretization models rely on the fact that the constant-strain triangular element stiffness will be calculated for points defined in the global coordinates, while the quadrilateral element stiffness is calculated using the natural coordinate system, which should be subsequently mapped into the global coordinate system.

## 3.5 Stress and Displacements

For the quadrilateral element mesh, the regular elements as well as the elements containing at least one enriched node but not cut by the crack contain regular distribution of the Gaussian integration points ($2\times2$, $3\times3$, ...). However for the elements cut by the crack more integration points are used to accurately integrate the stiffness along the edges of the discontinuity. More details regarding the Gaussian points for the elements cut by the crack are explained in Section 4.2.3.

The stress will be found for each Gaussian point in the mesh and then saved in one matrix along the global values of the Gaussian points. Since the element stiffness matrix will contain the extra degrees of freedom beside the regular degrees of freedom, the global stiffness matrix will contain all the degrees of freedom including the extra ones. Thus the displacement obtained will also contain the values of displacement for the extra degrees of freedom beside the regular degrees of freedom.

For example, when all the nodes in the quadrilateral element are regular then the displacement at any point inside the element will be:

$$u = u_1\varphi_1 + u_2\varphi_2 + u_3\varphi_3 + u_4\varphi_4 \qquad (3.23\text{-a})$$

$$v = v_1\varphi_1 + v_2\varphi_2 + v_3\varphi_3 + v_4\varphi_4 \qquad (3.23\text{-b})$$

where $\varphi_i$ is the shape function for node *I*.

But if the element contains the first node (node 1) enriched by the Heaviside enrichment function and this node is located below the crack, the displacement will be:

$$u = u_1\varphi_1 + u_2\varphi_2 + u_3\varphi_3 + u_4\varphi_4 - a_x\varphi_1 \qquad (3.24\text{-a})$$

$$v = v_1\varphi_1 + v_2\varphi_2 + v_3\varphi_3 + v_4\varphi_4 - a_y\varphi_1 \qquad (3.24\text{-b})$$

where $a_x$ and $a_y$ are the values obtained in the displacement vector which are referred to the extra degrees of freedom for this node. As another example, if the first node is enriched by the near tip 2 enrichment functions, then the displacement inside the element can be obtained as:

$$u = u_1\varphi_1 + u_2\varphi_2 + u_3\varphi_3 + u_4\varphi_4 + b1_x F_1\varphi_1 + b2_x F_2\varphi_1 + b3_x F_3\varphi_1 + b4_x F_4\varphi_1 \quad (3.25\text{-a})$$

$$v = v_1\varphi_1 + v_2\varphi_2 + v_3\varphi_3 + v_4\varphi_4 + b1_y F_1\varphi_1 + b2_y F_2\varphi_1 + b3_y F_3\varphi_1 + b4_y F_4\varphi_1 \quad (3.25\text{-b})$$

where $b1_x$, $b2_x$, $b3_x$, $b4_x$, $b1_y$, $b2_y$, $b3_y$ and $b4_y$ are the values obtained from the displacement vector along the extra degrees of freedom that belong to the node.

## 3.6 Conclusion

It can be concluded that XFEM is basically regular finite element with enrichment functions that are required to be added to some nodes in the mesh to account for the discontinuities. Thus it can easily be formulated in the framework of regular finite element method.

In XFEM, the mesh is generated before locating the discontinuities and thus there is no need to align the elements' edges along the crack faces or to use high density mesh in the crack tip region. The element partitioning is a good approach for the elements that were cut by the crack in order to accurately integrate the discontinuities along the two faces of the element.

# CHAPTER FOUR

# EXTENDED FINITE ELEMENT METHOD-IMPLEMENTATION

## 4.1 Introduction

As mentioned before, XFEM is a numerical technique for modeling discontinuities within the frame work of the standard finite elements by introducing discontinuous enrichment and crack tip enrichment functions. One is able to model the crack in isotropic linear elasticity problem using XFEM without the need to align the mesh with the crack surfaces which is the case in the regular finite element where the crack is required to be explicitly modeled. Using XFEM, quasi-static crack propagation can be handled without re-meshing.

This chapter discusses some of the key issues regarding computer implementation of XFEM. First the two-dimensional domain discretization before locating the crack is described. Then modeling the crack in two-dimensions implicitly by selecting the nodes for enrichment is discussed. Obtaining the stiffness matrix for the enriched elements is also explained. Finally the procedure for obtaining the first and second modes of the stress intensity factor is described.

Numerical examples including plate with crack located at different locations and inclined in different angles and cracks initiated from holes are provided to demonstrate the robustness of the XFEM. It has been shown the excellent agreement between the stress intensity factors obtained using XFEM and those obtained from exact analytical solutions.

## 4.2 Computer Implementations

The schematic diagram regarding implementation of the XFEM is shown in Figure 4.1. As it can be observed, numerical simulation using XFEM requires the following main components:

- Discretize the domain using regular finite element program.
- Obtain the global stiffness matrix and the global force vector.
- Locate the crack geometry (the crack is considered as a piecewise linear segment).
- Select the nodes for enrichment using the nodal enrichment scheme.
- Distinct the elements into regular elements, enriched elements not cut by the crack and elements cut by the crack.
- Obtain the element stiffness for the enriched elements and the elements cut by the crack.
- Assemble only the extra degrees of freedom from these elements into the previously obtained global stiffness matrix.
- Calculate the displacement vector (the displacement vector contains the extra degrees of freedom as well as the regular ones).

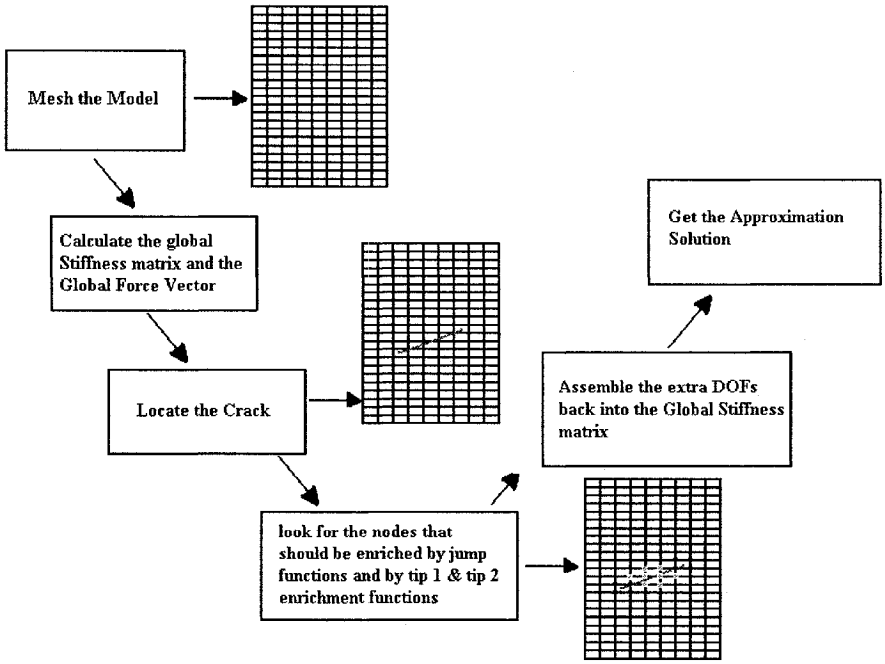


Figure 4.1: Schematic diagram for the XFEM technique

This Chapter describes in detail the issues regarding discretization of the domain using regular finite element mesh generator; selecting the nodes for enrichment through enrichment scheme; distinction of the elements into regular or enriched; and the procedure to obtain the stress intensity factor. Both quadrilateral elements and constant-strain triangular elements are used in the numerical examples. Here the implementation is described for the quadrilateral elements for sake of brevity. The same concepts are applicable for the triangular elements.

### 4.2.1 Domain discretization

As in XFEM the crack is not required to be explicitly aligned with the mesh, the mesh can be generated regardless of the crack location. The two-dimensional domain can be discretized using regular finite element mesh generator. When the domain is

discretized, the global stiffness matrix $[KK]$ and the force vector $\{ff\}$ are obtained using the regular finite element method.

### 4.2.2 Enrichment scheme

When the domain discretization is performed, the crack location is specified through its tip 1 and tip 2 coordinates; as the crack is considered as piecewise linear segment. Since the crack is arbitrary located and not aligned with the mesh, it is modeled implicitly by enriching the nodes that their support area is cut by the crack. To implement this task, the intersection points between the crack and the supports of each node are calculated. This is performed by exploiting the equations that represent both; the crack and the support edges.

To perform the enrichment scheme and to distinct the types of elements, two vectors are created. The first vector is called nodes_ID and its length is equal to the number of nodes in the mesh. The index for each element in the vector represents an equivalent node in the mesh and the value assigned to each element in the vector specifies the type of the equivalent node in the mesh. For instance, if nodes_ID(25) = 1 this means that the node 25 in the mesh is located above the crack and enriched by the discontinuity function. The list of the values and what they represent for the vector nodes_ID are itemized below:

0 Regular finite element node.

1 Node located above the crack and enriched by the discontinuity function.

-1 Node located below the crack and enriched by the discontinuity function.

10 Node located on the crack and enriched by the discontinuity function.

11 Node located in tip 1 field and enriched by the tip 1 enrichment functions.

22 Node located in tip 2 field and enriched by the tip 2 enrichment functions.

The second vector is called Elements_ID and its length is equal to the number of elements in the mesh. In similar the index for each element in the vector represents an equivalent element in the mesh and the value assigned to each element in the vector specifies the type of the equivalent element in the mesh. For instance, Elements_ID(43) = 1 means that the element 43 in the mesh is cut by the crack. Here is the list of the values and their representation for the vector Elements_ID:

0 Regular finite element

10 Enriched element and not cut by the crack

1 Element cut by the crack.

The enrichment scheme as shown in Figure 4.2 can be implemented by checking all the nodes in the mesh. The node $I$ will be enriched by tip 1 or tip 2 enrichment functions if it is located inside the geometrical enrichment field (i.e. if it is located inside circle centered at the crack tip and has the radius $R_{enrich}$). Then the appropriate value will be assigned to the element $I$ in the vector nodes_ID, that is nodes_ID( $I$ ) = (11 or 22). This is performed simply by checking the distance between node $I$ and the tip. If this distance is less than the radius of enrichment $R_{enrich}$, then it will be enriched.

The radius of enrichment is recommended to be related to the element edge length $h_e$ as $1.5h_e \leq R_{enrich} \leq 4.5h_e$. For smaller $R_{enrich}$, the results will not be accurate since fewer elements will bear the complete approximation solution, and for large $R_{enrich}$, excellent accuracy can be achieved, however this will increase the final degrees of freedom in an accelerated manner causing high computational cost. This is explained further in Section 4.5.

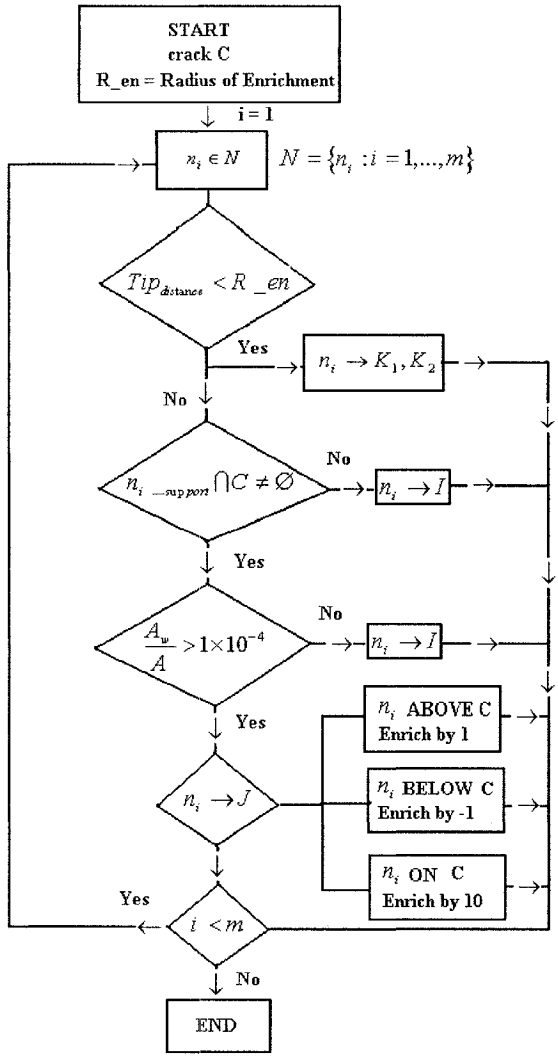


Figure 4.2: Flowchart for nodes enrichment

If the node $I$ is not enriched by the tip enrichment functions, the support area $\omega_I$ will be checked. If the support area is not cut by the crack, the node $I$ will be regular finite element node and an appropriate value will be assigned to the element $I$ in the vector nodes_ID (nodes_ID( $I$ ) = 0). If the support area is cut by the crack and the area criterion $\frac{A_w}{A} > 1\times10^{-4}$ is met ($A_w$ is the smallest area after the intersection and $A$ is the total support area) then the node $I$ will be enriched by the Heaviside discontinuity

function and an appropriate value will be assigned to the element $I$ in the vector nodes_ID based on the node $I$ location (above, below or on the crack). If the area criterion is not satisfied, the node $I$ will be treated as regular finite element node and an appropriate value will be assigned to the element $I$ in the vector nodes_ID.

Checking if the node $I$ is located above, below or on the crack can be easily executed using the following equation:

$$\Delta = (x_1 - x)(y_2 - y) - (x_2 - x)(y_1 - y) \tag{4.1}$$

where $(x_1,y_1)$ is the first intersection point of the nodal support and $(x_2,y_2)$ is the second one, $x$ and $y$ are the coordinates of node $I$. Now if $\Delta > \varepsilon$, the node $I$ is located above the crack, if $\Delta < -\varepsilon$, the node $I$ is located below the crack and if $-\varepsilon \leq \Delta \leq \varepsilon$, the node $I$ is located on the crack. Here $\varepsilon$ is a tolerance value usually set at $1\times10^{-6}$ of the element edge length.

When the enrichment scheme is performed, it is possible to distinct the type of elements in the mesh (regular or enriched). The element $M$ is treated as regular finite element if all its nodes are considered as regular finite element nodes, in this case the value 0 will be assigned to the element $M$ in the vector Elements_ID. If the element $M$ has at least one enriched node, provided that it is not cut by the crack, the element is treated as enriched element and the value 10 will be assigned to the element $M$ of the vector Elements_ID. Finally, if the element $M$ is cut by the crack, the value 1 will be assigned to the element $M$ of the vector Elements_ID.

### 4.2.3 Element stiffness matrix and element partitioning

As mentioned in the previous section, three types of elements exist in a domain with pre-existent crack. Different procedure is required to find the element stiffness matrix for each type. For the regular finite elements, it is not required to evaluate the element stiffness matrix as it has already been calculated and assembled to the global stiffness matrix. This has already been performed before locating the crack using the regular finite element framework.

For the elements that contain at least one enriched node, the contribution in the stiffness matrix due to the classical degrees of freedom as well as the extra degrees of freedom are evaluated, both contributions are stored in a single element stiffness matrix. For this type of elements the discontinuity enrichment function $H$ is related to the node itself. If the enriched node is located above the crack then the enrichment function $H$ for this node will be 1, and if the enriched node is located below the crack, then the enrichment function $H$ for this node will be -1. But if the enriched node is located on the crack, the value of the enrichment function $H$ will be 1 when calculating the stiffness for the element located above the crack and -1 when calculating the stiffness for the element located below the crack.

The elements cut by the crack require more Gaussian points to accurately integrate the discontinuities along the two faces of the element. Here the element cut by the crack is divided into sub-elements that have the triangular shapes where the crack is aligned with the edge of one triangle for the upper part of the element and with the edge of another triangle for the lower part. This technique is called the element partitioning.

Figure 4.3 shows the sub-triangles and the Gaussian points for an element cut by the crack.

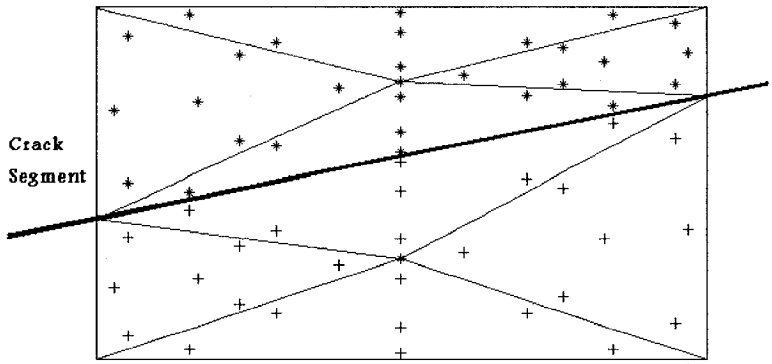


Figure 4.3: Gaussian points for the partitioned element

Depending on the crack location, the sub-elements are established for the elements cut by the crack. Each sub-element contains 7-integration points which are defined in the local coordinates of the sub-elements (triangles). Thus mapping is required to convert the integration points from the local coordinates of the sub-elements to the global coordinates and then back to the local coordinates of the parent element. The function that implements this mapping is presented in Appendix B.

It is good to emphasize at this point that the value of the enrichment function $H$ for the elements cut by the crack is dependant on the location of the integration points and independent on the location of the node itself (i.e. above or below the crack). In other words, if the integration point is located above the crack, all the nodes of the element will be enriched by 1 even if some of these nodes are located below the crack.

### 4.2.4 Assembly procedure

In the regular finite element method, the assembly procedure is straight forward since the index used to assemble the element stiffness matrix to the global stiffness matrix is related to the number of the node and the domain dimension (2-D or 3-D). For example, the node 50 in two-dimensional mesh can have the index 99 for its $x$-coordinate and 100 for its $y$-coordinate.

In the XFEM, the enriched nodes will contain extra degrees of freedom. These degrees of freedom are dependant on the enrichment function. That is, the node enriched by the discontinuity function will contain two extra degrees of freedom, while the node enriched by the tip enrichment function will contain eight extra degrees of freedom. Hence, each element in the mesh will contain different total degrees of freedom depending on the number of the enriched nodes and their enrichment functions. If the quadrilateral element has only one node enriched by the tip enrichment function and the rest are regular, the total degrees of freedom for the element will be 16 consisting of 8 regular degrees of freedom and 8 extra degrees of freedom resulted from the enriched node.

For assembly purposes in XFEM a vector called index_XFEM is established. The purpose of this vector is to give an index for the extra degrees of freedom, while the regular degrees of freedom will be indexed using the same procedure in the regular finite element. Using this vector, it can be assured that the global stiffness matrix with the extra degrees of freedom is properly assembled. This global stiffness matrix can be recalled as needed in the case of the crack growth problems.

After indexing the extra degrees of freedom in the mesh, the assembly procedure is continued for the second and third type of elements (enriched elements not cut by the crack and elements cut by the crack) by incorporating only the extra degrees of freedom to the global stiffness matrix of the regular elements in the background mesh. Appendix B contains two developed Matlab programs that can be used to obtain the total degrees of freedom for the element and the indexing values for the extra degrees of freedom, respectively.

## 4.3 Evaluation of the Stress Intensity Factor (SIF)

The stress intensity factor is a linear elastic fracture mechanics parameter that relates remote load, crack size and structural geometry. Exact solutions for the stress intensity factors are available for many crack geometries and can be used to validate the stress intensity factor evaluated numerically using XFEM.

The numerical solution for the stress intensity factors are computed using XFEM for different problems, and the results are compared with available analytical solutions to validate the accuracy of the XFEM for modeling the cracks and the crack growth in the mechanical structures. In this work, the stress intensity factors are computed using the domain forms of the interaction integral [28-31]. It is assumed that the plastic zone around the crack tip is very small and linear elastic fracture mechanics concept is valid.

The interaction integral is obtained from the *J*-integral which is defined as the line integral defined around a contour $\Gamma$ as shown in Figure 4.4 and characterizes the stress-strain field around the crack front. If the LEFM is applicable, then the *J*-integral represents the energy release rate at the crack tip during the crack growth. In general the *J*-integral can be written as:

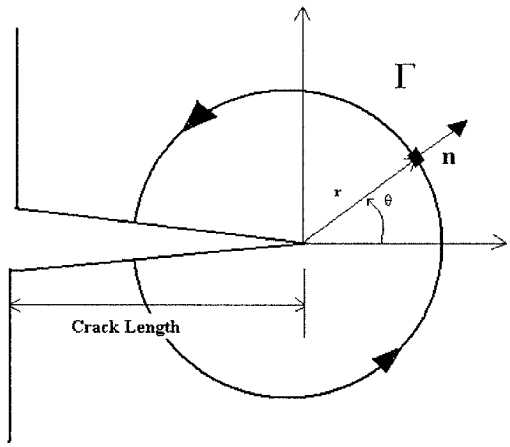


Figure 4.4: J-integral contour

$$J = \int_{\Gamma}\left[\frac{1}{2}(\sigma_{ij})(\varepsilon_{ij})\delta_{1j} - (\sigma_{ij})\frac{\partial(u_i)}{\partial x_1}\right] n_j d\Gamma \tag{4.2}$$

where $\sigma_{ij}$ is the stress tensor, $\varepsilon_{ij}$ is the strain tensor, $u_i$ is the displacement vector and $n_j$ is unit vector outward normal to the contour $\Gamma$. For general two-dimensional mixed-mode case the relationship between the *J*-integral and mode-*I* and mode-*II* of the stress intensity factors can be written as [28]:

$$J = \frac{K_I^2}{E^*} + \frac{K_{II}^2}{E^*} \tag{4.3}$$

where $E^*$ is defined in terms of $E$ (Modulus of elasticity) and $\upsilon$ (Poisson's ratio) as:

$$E^* = \begin{cases} E & \text{Plane stress} \\ \dfrac{E}{1-\upsilon^2} & \text{Plane strain} \end{cases} \tag{4.4}$$

Two states of a cracked body are considered. State 1 $(\sigma_{ij}^{(1)}, \varepsilon_{ij}^{(1)}, u_i^{(1)})$ corresponds to the present state and state 2 $(\sigma_{ij}^{(2)}, \varepsilon_{ij}^{(2)}, u_i^{(2)})$ is an auxiliary state which will be chosen as

the asymptotic fields for pure mode-*I* or mode-*II*. The *J*-integral for the sum of the two states is:

$$J^{(1+2)} = \int_{\Gamma}\left[\frac{1}{2}(\sigma_{ij}^{(1)}+\sigma_{ij}^{(2)})(\varepsilon_{ij}^{(1)}+\varepsilon_{ij}^{(2)})\delta_{1j} - (\sigma_{ij}^{(1)}+\sigma_{ij}^{(2)})\frac{\partial(u_i^{(1)}+u_i^{(2)})}{\partial x_1}\right] n_j d\Gamma \quad (4.5)$$

Now expanding the terms, the *J*-integral for the sum of the two states will be written as:

$$J^{(1+2)} = J^{(1)} + J^{(2)} + I^{(1,2)} \quad (4.6)$$

where

$$I^{(1,2)} = \int_{\Gamma}\left[W^{(1,2)}\delta_{1j} - \sigma_{ij}^{(1)}\frac{\partial u_i^{(2)}}{\partial x_1} - \sigma_{ij}^{(2)}\frac{\partial u_i^{(1)}}{\partial x_1}\right] n_j d\Gamma \quad (4.7)$$

in which

$$W^{(1,2)} = \frac{1}{2}\left[\sigma_{ij}^{(1)}\varepsilon_{ij}^{(2)} + \sigma_{ij}^{(2)}\varepsilon_{ij}^{(1)}\right] = \sigma_{ij}^{(1)}\varepsilon_{ij}^{(2)} = \sigma_{ij}^{(2)}\varepsilon_{ij}^{(1)} \quad (4.8)$$

is the interaction strain energy from the two states. Based on Eq. (4.3) the *J*-integral for the sum of the two states can also be represented as:

$$J^{(1+2)} = \frac{(K_I^{(1)}+K_I^{(2)})^2}{E^*} + \frac{(K_{II}^{(1)}+K_{II}^{(2)})^2}{E^*} \quad (4.9)$$

rearranging the terms in Eq. (4.9) yields:

$$J^{(1+2)} = J^{(1)} + J^{(2)} + \frac{2}{E^*}(K_I^{(1)}K_I^{(2)} + K_{II}^{(1)}K_{II}^{(2)}) \quad (4.10)$$

now equating Eq. (4.6) and Eq. (4.10) leads to the following relationship:

$$I^{(1,2)} = \frac{2}{E^*}(K_I^{(1)}K_I^{(2)} + K_{II}^{(1)}K_{II}^{(2)}) \quad (4.11)$$

The contour integral in Eq. (4.7) is not in a form well suited for finite element calculations. Therefore, it is recasted into an equivalent domain form by multiplying the integrand by smooth weighting function *q(x)* which takes the value of unity on the crack

tip and vanish on a prescribed contour $C$. Assuming the crack faces are traction free and straight in the region $A$ that is bounded by the contour $C$, the interaction integral can be rewritten in the domain form using the divergence theorem as [30, 31]:

$$I^{(1,2)} = \int_A \left[ \sigma_{ij}^{(1)} \frac{\partial u_i^{(2)}}{\partial x_1} + \sigma_{ij}^{(2)} \frac{\partial u_i^{(1)}}{\partial x_1} - W^{(1,2)} \delta_{1j} \right] \frac{\partial q}{\partial x_j} dA \tag{4.12}$$

If the auxiliary state 2 is considered as pure mode-*I* asymptotic fields, then $K_I^{(2)} = 1$ and $K_{II}^{(2)} = 0$. Subsequently using Eq. (4.11), the first mode of the stress intensity factor $K_I$ can be obtained as:

$$K_I = \frac{E^*}{2} I^{(1,Mode-I)} \tag{4.13}$$

and the stresses and displacements for state 2 can be obtained from Eq. (2.8) and (2.9) as:

$$\begin{Bmatrix} \sigma_{xx}^{(2)} \\ \sigma_{yy}^{(2)} \\ \tau_{xy}^{(2)} \end{Bmatrix} = \frac{1}{\sqrt{2\pi r}} \begin{Bmatrix} \cos\frac{\theta}{2}(1 - \sin\frac{\theta}{2}\sin\frac{3\theta}{2}) \\ \cos\frac{\theta}{2}(1 + \sin\frac{\theta}{2}\sin\frac{3\theta}{2}) \\ \cos\frac{\theta}{2}\sin\frac{\theta}{2}\cos\frac{3\theta}{2} \end{Bmatrix} \tag{4.14}$$

$$\begin{Bmatrix} u_1^{(2)} \\ u_2^{(2)} \end{Bmatrix} = \frac{1}{2\mu}\sqrt{\frac{r}{2\pi}} \begin{Bmatrix} \cos\frac{\theta}{2}\left[\kappa - 1 + 2\sin^2\frac{\theta}{2}\right] \\ \sin\frac{\theta}{2}\left[\kappa + 1 - 2\cos^2\frac{\theta}{2}\right] \end{Bmatrix} \tag{4.15}$$

where $\mu$ is the shear modulus and $\kappa = (3-\upsilon)/(1+\upsilon)$ for plane stress and $\kappa = 3 - 4\upsilon$ for plane strain.

In similar way, to obtain the second mode of the stress intensity factor $K_{II}$ it is required to set the auxiliary state 2 as pure mode-*II* asymptotic fields. This is achieved by

setting $K_{II}^{(2)} = 1$ and $K_{I}^{(2)} = 0$. Then using Eq. (4.11), we can obtain the second mode of the stress intensity factor $K_{II}$ as:

$$K_{II} = \frac{E^*}{2} I^{(1,Mode-II)} \tag{4.16}$$

and the stresses and displacements for state 2 in this case can be obtained from Eqs. (2.9) and (2.10) as:

$$\begin{Bmatrix} \sigma_{xx}^{(2)} \\ \sigma_{yy}^{(2)} \\ \tau_{xy}^{(2)} \end{Bmatrix} = \frac{1}{\sqrt{2\pi r}} \begin{Bmatrix} -\sin\frac{\theta}{2}(2+\cos\frac{\theta}{2}\cos\frac{3\theta}{2}) \\ \sin\frac{\theta}{2}\cos\frac{\theta}{2}\cos\frac{3\theta}{2} \\ \cos\frac{\theta}{2}(1-\sin\frac{\theta}{2}\sin\frac{3\theta}{2}) \end{Bmatrix} \tag{4.17}$$

$$\begin{Bmatrix} u_1^{(2)} \\ u_2^{(2)} \end{Bmatrix} = \frac{1}{2\mu}\sqrt{\frac{r}{2\pi}} \begin{Bmatrix} \sin\frac{\theta}{2}\left[\kappa+1+2\cos^2\frac{\theta}{2}\right] \\ -\cos\frac{\theta}{2}\left[\kappa-1-2\sin^2\frac{\theta}{2}\right] \end{Bmatrix} \tag{4.18}$$

now expanding each term of Eq. (4.12) yields:

$$I^{(1,2)} = \int_A h dA \tag{4.19}$$

where

$$h = h_1 + h_2 + h_3 + h_4 + h_5 + h_6 - h_7 - h_8 \tag{4.20}$$

The terms $h_1, \ldots, h_8$ for both plane stress and plain strain conditions are derived in Appendix A.

More discussion of methods and solution techniques for finding the stress intensity factors for different type of problems may be found in Rooke [16], Broek [32] and Parker [33].

## 4.4 Illustrative Examples

Numerous examples including plates with edge crack, centered crack, two centered cracks initiated from hole and crack inclined in different angles are studied using both quadrilateral and constant-strain triangular element mesh. The main objective in this section is to validate the numerical results obtained by XFEM. For this purpose, stress intensity factors for different problems will be obtained using XFEM for both quadrilateral and triangular element mesh and compared with the exact solutions available. Once this objective is achieved and the XFEM is validated, the crack growth problems will be simulated for different problems using XFEM.

In all problems investigated in this section, the thickness of the plate is selected as $t$ = 5 mm (except Section 4.4.2) and the material used is 304 Stainless Steel with modulus of elasticity $E$ = 190 GPa, modulus of rigidity $G$ = 73.1 GPa and Poisson's ratio $\upsilon = 0.305$. The yield strength for the stainless steel is $\sigma_{YS} = 276\ MPa$, the fracture toughness where the failure occurs is $K_{IC} = 66\ MPa\sqrt{m}$ and the threshold stress intensity factor is $K_{threshold} = 4.6\ MPa\sqrt{m}$. Plane stress conditions and linear elastic fracture mechanics are assumed.

### 4.4.1 Plate with edge crack under uniform tensile loading

Consider a rectangular plate with dimensions $10 \times 20$ cm and thickness of 5 mm as shown in Figure 4.5. The plate has a crack with length $a$ = 5 cm located at the mid height and is subjected to uniform tensile stress of 10 MPa.

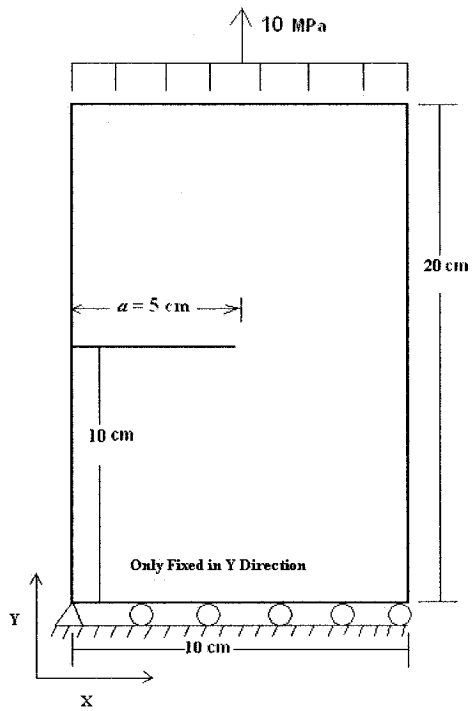


Figure 4.5: Plate with edge crack under tensile loading

The exact solution for the first mode stress intensity factor can be written as [34]:

$$K_I = C\sigma\sqrt{a\pi} \tag{4.21}$$

where

$$C = 1.12 - 0.231\left(\frac{a}{W}\right) + 10.55\left(\frac{a}{W}\right)^2 - 21.72\left(\frac{a}{W}\right)^3 + 30.39\left(\frac{a}{W}\right)^4 = 2.8264 \tag{4.22}$$

$a$ is the length of the crack, and $W$ is the width of the plate.

Using provided dimensions, stress intensity factor for mode-$I$ can be found as:

$$K_I = 2.8264 \times 10\sqrt{5 \times 10^{-2} \times \pi} = 11.202\ MPa\sqrt{m} \tag{4.23}$$

Table 4.1 provides the normalized first mode stress intensity factor $K_I$ obtained numerically using XFEM with respect to the exact solution for different element mesh types and sizes and different enrichments' radiuses on the crack tip.

Table 4.1: Normalized $K_I$ for plate with edge crack under uniform tensile loading

| Radius of Enrichment / Mesh | 1.5 $h_e$ | | 2.5 $h_e$ | | 3.5 $h_e$ | |
|---|---|---|---|---|---|---|
| | **Quad** | **Tri** | **Quad** | **Tri** | **Quad** | **Tri** |
| **SDOF Quad=462 SDOF Tri = 468** | 0.9592 | 0.9125 | 0.9680 | 0.9288 | 0.9731 | 0.9401 |
| **SDOF Quad = 1722 SDOF Tri = 1724** | 0.9851 | 0.9412 | 0.9893 | 0.9520 | 0.9915 | 0.9578 |

The SDOF stands for the total system degrees of freedom for the background mesh. As it can be realized for comparable SDOF, the quadrilateral elements (Quad) provide more accurate results compared to the triangular elements (Tri). Also, it can be seen that the accuracy generally increases when the radius of enrichment increases. However this will increase the enrichment degrees of freedom which may increase the computational cost. For instance, for the quadrilateral elements in the second row of Table 4.1 the final degrees of freedom including the enrichment increases from 1812 for the radius of enrichment $R_{enrich}$ = 1.5 $h_e$ to 2032 for $R_{enrich}$ = 3.5 $h_e$. Figures 4.6 shows the tensile stress distribution in the plate along $y$ direction resulted from the XFEM solution for the quadrilateral element mesh for the second row in Table 4.1 with radius of enrichment 3.5 $h_e$.

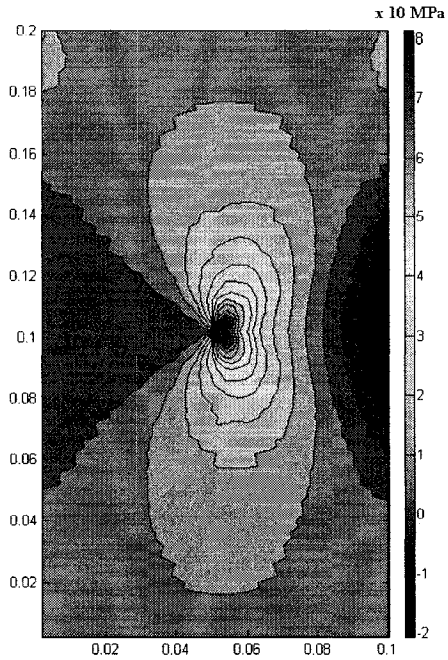


Figure 4.6: Tensile stress distribution for plate with edge crack under uniform tensile loading (units in m)

### 4.4.2 Plate with edge crack under uniform shear loading

The plate with dimensions $7 \times 16$ in. ($17.78 \times 40.64$ cm) and thickness of $t = 1$ in. (2.54 cm) has a crack with length of $a = 3.5$ in. (8.89 cm) located in the mid height of the plate as shown in Figure 4.7. The plate is under uniform shear stress of 1 psi (6.89 kPa) acting on the upper edge.

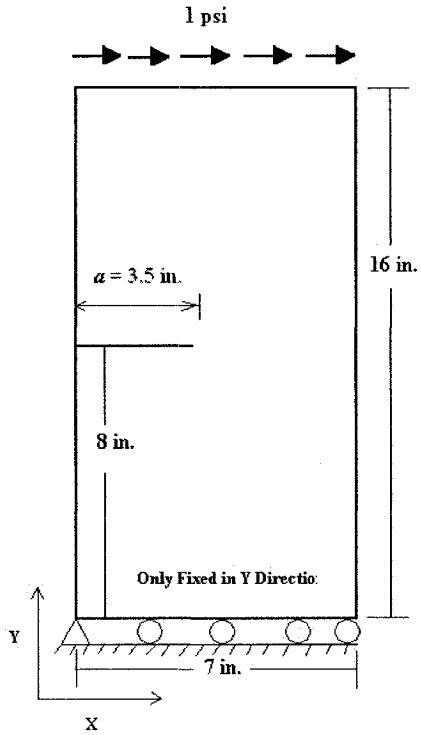


Figure 4.7: Plate with edge crack under shear loading

The exact solution for stress intensity factor for mode-*I* and mode-*II* is [28]:

$$K_I = 34.0\ psi\sqrt{in} = 37.335\ kPa\sqrt{m}, \quad K_{II} = 4.55\ psi\sqrt{in} = 4.996\ kPa\sqrt{m} \quad (4.24)$$

The discretization model is obtained using quadrilateral element mesh (14x32 elements), with a total system degrees of freedom 990. Different radiuses of enrichments are performed. The XFEM simulations are normalized with respect to the exact solution and are presented in Table 4.2 for both the first and second modes of the stress intensity factor.

Table 4.2: Normalized results for $K_I$ and $K_{II}$ for plate with edge crack under uniform shear loading

| Radius of Enrichment / Normalized $K_I$ and $K_{II}$ | 1.5 $h_e$ | 2.5 $h_e$ | 3.5 $h_e$ |
|---|---|---|---|
| **Normalized $K_I$** | 0.9796 | 0.9860 | 0.9897 |
| **Normalized $K_{II}$** | 0.9838 | 0.9854 | 0.9865 |

It can be realized that the accuracy increases as the radius of enrichment increases. However as mentioned before, this will increase the enrichment degrees of freedom causing more computational time. For this problem the total system degrees of freedom including the enrichment ones increases from 1074 for radius of enrichment 1.5 $h_e$ to 1294 for radius of enrichment 3.5 $h_e$. Figure 4.8 shows the shear stress distribution in the plate resulted from the XFEM simulation for the radius of enrichment 3.5 $h_e$.

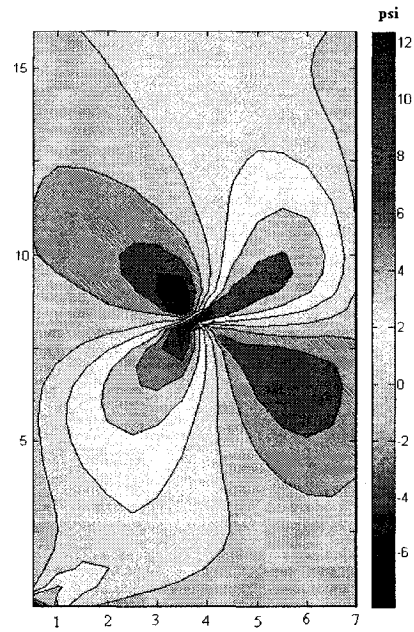


Figure 4.8: Shear stress distribution for plate with edge crack under uniform shear loading (units in in.)

### 4.4.3 Plate with central crack under uniform tensile loading

The plate for this problem has similar dimensions and thickness of problem 4.4.1 and is under the same tensile loading of 10 MPa. However in this problem the crack of half length $a$ = 2 cm is located at mid height and 3 cm away from the edges as shown in Figure 4.9.

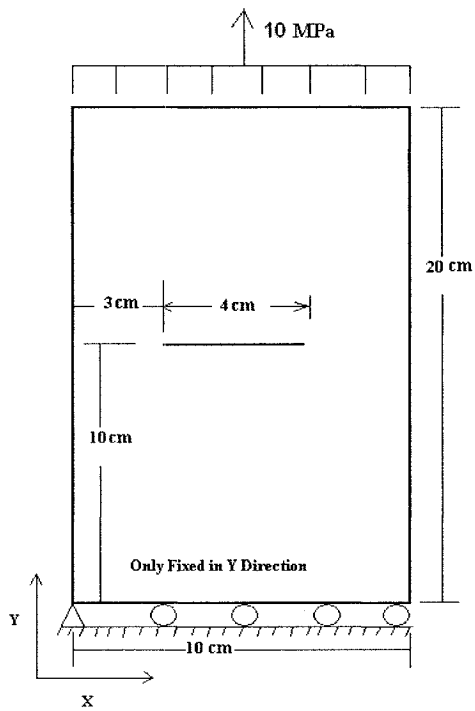


Figure 4.9: Plate with central crack under uniform tensile loading

For this case the stress intensity factor for mode-*I* is [35]:

$$K_I = C\sigma\sqrt{\pi a} \tag{4.25}$$

where

$$C = \frac{1 - 0.5\frac{a}{b} + 0.326\left(\frac{a}{b}\right)^2}{\sqrt{1-\frac{a}{b}}} \tag{4.26}$$

where $a$ is the half crack length, $b$ is the half width of the plate. Substituting the dimensions of the plate and the geometry of the crack into Eq. (4.25), we can find:

$$K_I = 1.1001 \times 10\sqrt{\pi \times 2 \times 10^{-2}} = 2.7575\ MPa\sqrt{\text{m}} \tag{4.27}$$

Table 4.3 provides the normalized first mode stress intensity factor $K_I$ obtained using XFEM for different mesh refinements and different geometrical enrichment radiuses for both quadrilateral and triangular elements with respect to the analytical solution.

Table 4.3: Normalized $K_I$ for plate with central crack under uniform tensile loading

| Radius of Enrichment / Mesh | 1.5 $h_e$ | | 2.5 $h_e$ | | 3.5 $h_e$ | |
|---|---|---|---|---|---|---|
| | **Quad** | **Tri** | **Quad** | **Tri** | **Quad** | **Tri** |
| **SDOF Quad=462 SDOF Tri = 468** | 0.9861 | 0.9327 | — | — | — | — |
| **SDOF Quad = 1722 SDOF Tri = 1724** | 1.001 | 0.9708 | 1.002 | 0.9744 | 1.003 | 0.9815 |

As it can be seen from this table, again more accurate results can be obtained from XFEM using quadrilateral elements compared to triangular elements. Also, as expected the accuracy increases by increasing the radius of enrichment, but this subsequently increase the enrichment degrees of freedom which consequently increase the computational cost. It should be mentioned that it is not possible to increase the radius of enrichment $R_{enrich} > 2$ cm to prevent the tip enrichment overlapping between tip 1 and tip 2, the reason why some cells in Table 4.3 are left empty. For the quadrilateral element in the second row of the Table 4.3 the final degrees of freedom including the enrichment

ones increases from 1876 for radius of enrichment of 1.5 $h_e$ to 2316 for radius of enrichment of 3.5 $h_e$. Figure 4.10 shows the tensile stress distribution in the plate along $y$ direction for the quadrilateral element mesh for the second row in Table 4.3 with radius of enrichment 3.5 $h_e$.

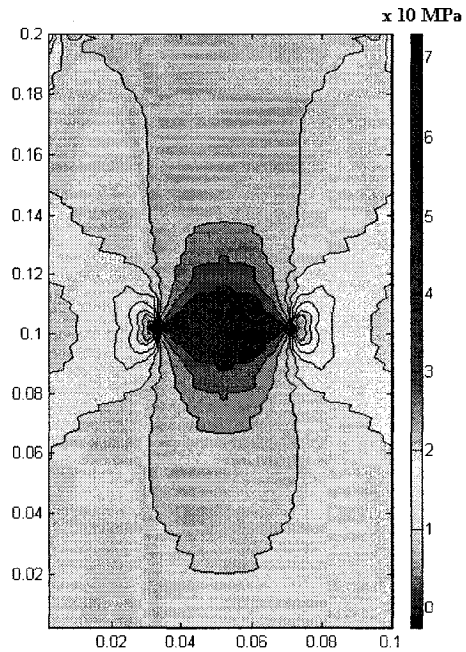


Figure 4.10: Stress distributions for plate with central crack under uniform tensile loading (units in m)

### 4.4.4 Plate with two cracks initiated from central hole under uniform tensile loading

In this problem similar plate studied in section 4.4.3 is considered. However the plate is under uniform tensile loading of 45 MPa and has a central hole with radius of 2.5 cm and two cracks with length $a$ = 4 cm. as shown in Figure 4.11

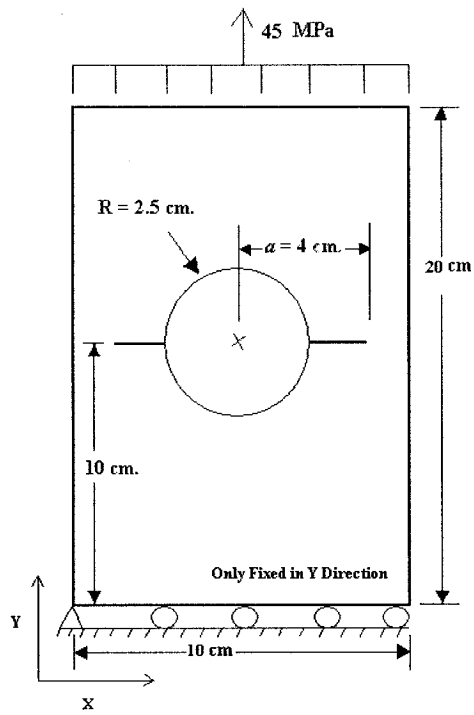


Figure 4.11: Plate with two cracks initiated from central hole under uniform tensile loading

The exact stress intensity factor for this problem is $K_I = C\sigma\sqrt{\pi a}$ in which $C$ is geometrical coefficient found from Figure 4.12 as $C$ = 2.2. Considering the provided dimensions, we obtain:

$$K_I = 2.2 \times 45\sqrt{\pi \times 4 \times 10^{-2}} = 35.095 \text{ MPa}\sqrt{\text{m}} \qquad (4.28)$$

Triangular element has been used to mesh the plate as shown in Figure 4.13. Using XFEM the result for stress intensity factors found to be $K_I = 33.4 \text{ MPa}\sqrt{\text{m}}$ which is in close agreement with the analytical result ($error \approx 4.83\%$). Figure 4.14 shows the tensile stress distribution in the plate along $y$ direction.

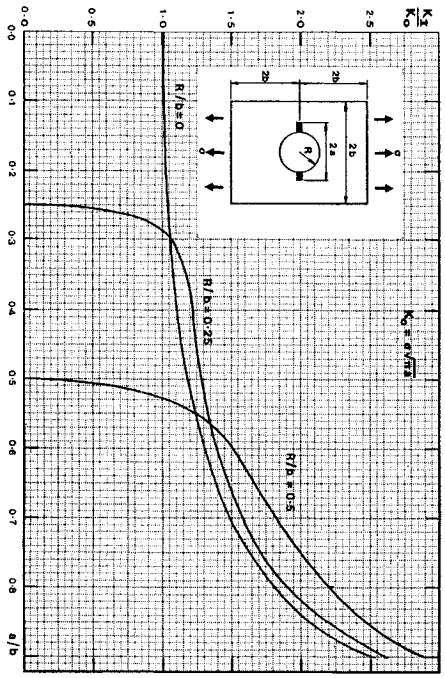


Figure 4.12: The geometrical coefficient C for plate with two cracks initiated from central hole [36]

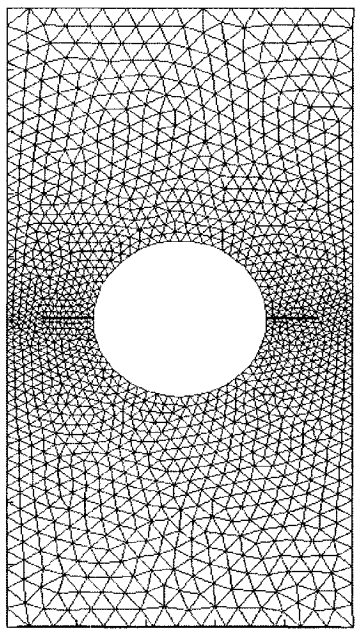

Figure 4.13: Background mesh for plate with central hole

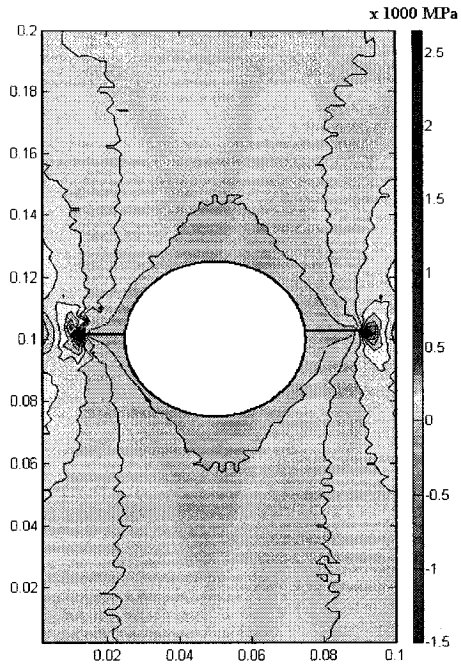


Figure 4.14: Stress distributions for plate with two cracks initiated from central hole under uniform tensile loading (units in m)

### 4.4.5 Plate with crack inclined with angle $\beta$ under uniform tensile loading

This section discusses the problems in which the crack is inclined in different angles. This will further confirm the robustness and validation of the XFEM since arbitrary locations for the crack tips require arbitrary nodal enrichments.

The plate for this problem has the dimensions of $20 \times 20$ cm and thickness of $t$ = 5 mm with half crack length of $a$ = 1.5 cm centered in the plate and inclined with angle $\beta$ as shown in Figure 4.15. The plate is under uniform tensile loading acting on the upper

edge resulting in stress of magnitude of $\sigma_y = 10\ MPa$. The domain is discretized using the quadrilateral elements.

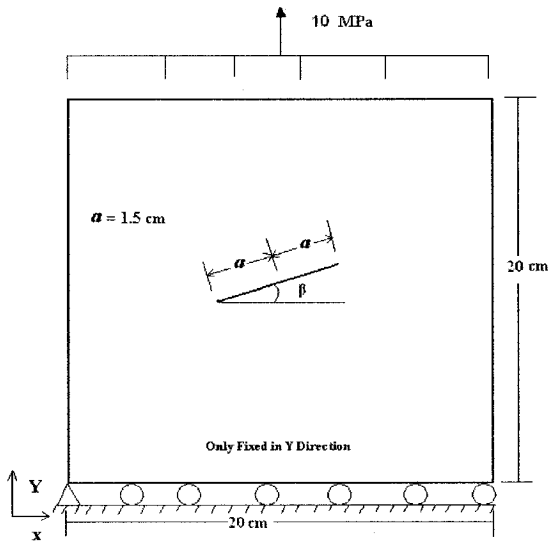


Figure 4.15: Plate with crack inclined with angle $\beta$

As the plate dimensions are large in comparison to the crack length, thus the analytical solution given for infinite plate for the first and second modes of the stress intensity factor can be used [28]:

$$K_I = \sigma\sqrt{\pi a}\cos^2(\beta)$$
$$K_{II} = \sigma\sqrt{\pi a}\sin(\beta)\cos(\beta) \qquad (4.29)$$

Tables 4.4 and 4.5 provide the normalized values for the first and second modes of the stress intensity factor obtained using XFEM with respect to the analytical solution for different angles $\beta$, respectively. The radius of enrichment is considered constant for all cases ($R_{enrich}$ = 1 cm).

Table 4.4: Normalized $K_I$ for plate with crack inclined at different angles $\beta$ under uniform tensile loading

| **Mesh** | $\beta = 15^0$ | $\beta = 30^0$ | $\beta = 45^0$ | $\beta = 60^0$ |
|---|---|---|---|---|
| **SDOF = 882** | 0.9711 | 0.9783 | 0.9733 | 0.9869 |
| **SDOF = 3362** | 0.9861 | 0.9880 | 1.008 | 1.008 |

Table 4.5: Normalized $K_{II}$ for plate with crack inclined with different angles $\beta$ under uniform tensile loading

| **Mesh** | $\beta = 15^0$ | $\beta = 30^0$ | $\beta = 45^0$ | $\beta = 60^0$ |
|---|---|---|---|---|
| **SDOF = 882** | 0.9368 | 0.9393 | 0.9433 | 0.9453 |
| **SDOF = 3362** | 0.9791 | 0.9572 | 0.9895 | 0.9825 |

As it can be realized from Tables 4.4 and 4.5, more accurate results can be achieved using finer mesh. Also, it should be emphasized again that it is not possible to use radius of enrichment greater than the half length of the crack to prevent the tip enrichment overlapping between the enrichment fields of tips 1 and 2.

Figures 4.16 shows the tensile stress distribution in the plate along $y$ direction for angle of $\beta = 45^0$.

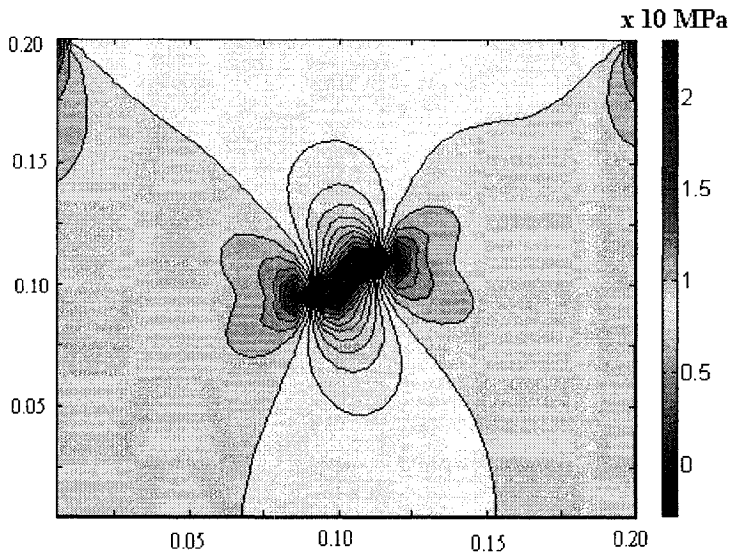


Figure 4.16: Stress distribution in plate with central crack inclined at $\beta = 45^0$ under uniform tensile loading (units in m)

Figure 4.17 shows the comparison between stress intensity factors for mode-*I* and mode-*II* obtained numerically using XFEM and analytical results for different crack inclined angles with fixed crack half length $a$ = 1.5 cm.

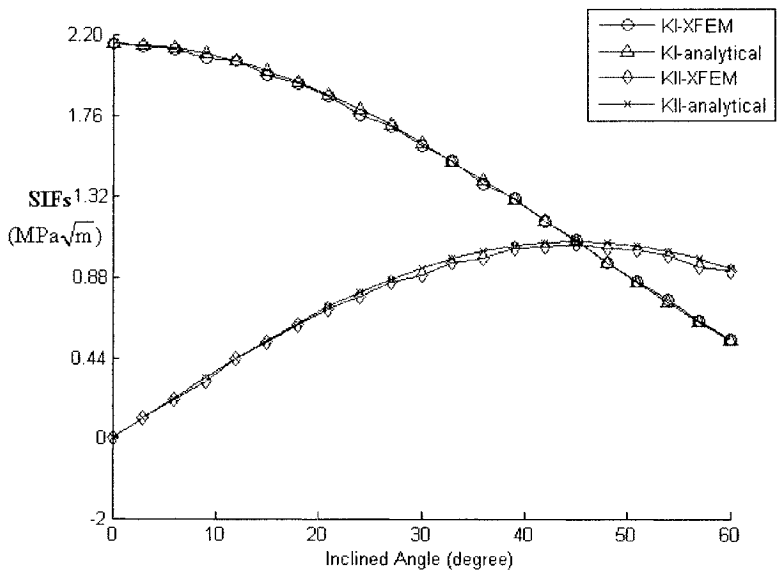


Figure 4.17: SIFs for plate with fixed crack length inclined in different angles

Figures 4.18 and 4.19 also show the comparison between stress intensity factors obtained numerically using XFEM and analytical results for crack with inclined angles of $15^{o}$ and $45^{o}$ respectively and different crack half length.

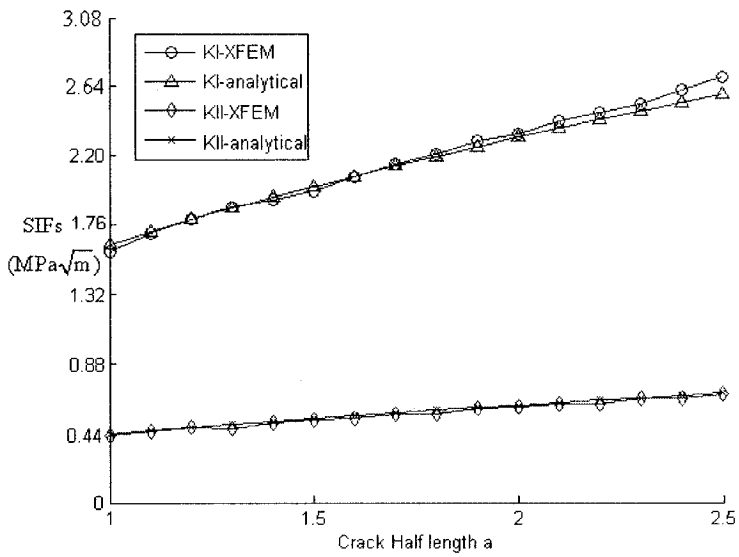


Figure 4.18: SIFs for plate with different cracked half lengths a (in cm) inclined in $15^{o}$.

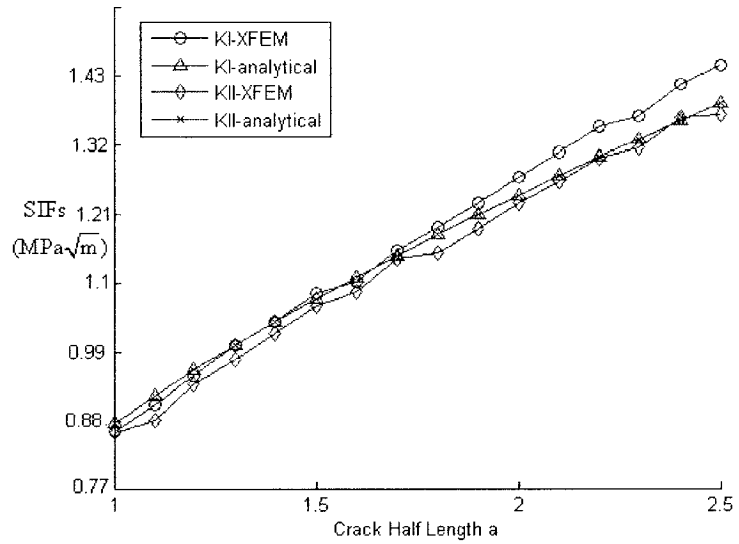


Figure 4.19: SIFs for plate with different cracked half lengths a (in cm) inclined in $45^{o}$.

As it can be realized from these figures, very good agreement exists between SIFs obtained using XFEM and analytical results confirming the robustness and accuracy of the developed XFEM formulation.

## 4.5 Radius of Enrichment and System Degrees of Freedom Relationship

As noted from the results for the problems discussed in section 4.4, the accuracy of the results increases as the radius of enrichment increases. However this will increase the enriched degrees of freedom in the system in an accelerated manner. The magnitude of the radius of enrichment is related with the element edge length $h_e$ used in the mesh and is recommended to be $1.5h_e \leq R_{enrich} \leq 4.5h_e$, as described below.

For the lower limit of the radius of enrichment, let us assume the crack tip is in the position shown in Figure 4.20. To enrich the four nodes of the element containing the crack tip the radius of enrichment $R_{enrich}$ should be $R_{enrich} \geq \sqrt{2}h_e \approx 1.414h_e$. Thus $R_{enrich} \geq 1.5h_e$ is good approximation.

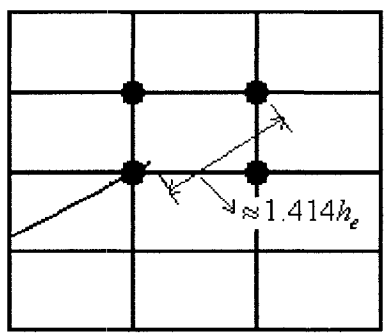


Figure 4.20: Radius of enrichment lower limit

As mentioned in section 4.2.4, each node in two-dimensional domain enriched by the tip enrichment functions will add 8 degrees of freedom to the total degrees of freedom, whereas the node enriched by the discontinuity function will add only 2 degrees of freedom. Thus, any node selected to be enriched by the tip function when the radius of enrichment increases will add 8 degrees of freedom to the total degrees of freedom. Figure 4.21 shows relationship between the radius of enrichment and the final degrees of freedom for the problem discussed in section 4.4.1 where the initial degrees of freedom before selecting the nodes for enrichment are 1722.

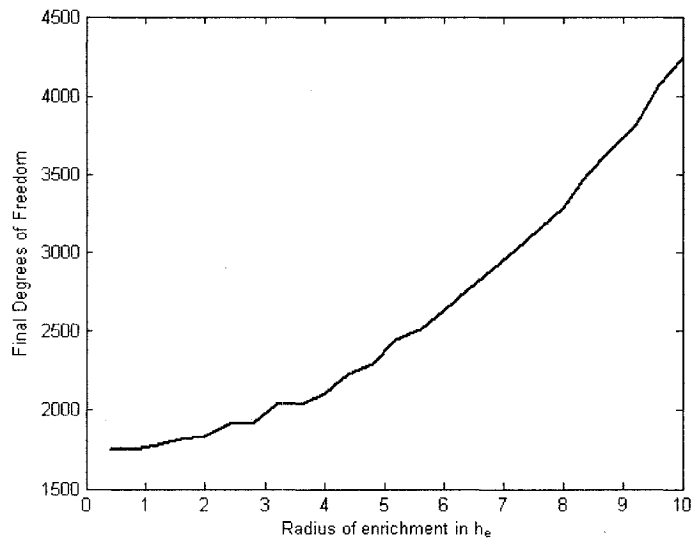


Figure 4.21: Final degrees of freedom versus radius of enrichment

It can be realized that the total degrees of freedom increase exponentially with the increase of the radius of enrichment. This comparison is for plate with edge crack and thus only one tip is involved in the tip enrichments. For central crack where both tips are

involved and for three-dimensional problems, the final degrees of freedom will increase even faster as the radius of enrichment increases causing high computational cost.

## 4.6 Conclusion

The computer implementation for modeling cracks in XFEM is performed using a vector to define the nodal types (enriched or regular finite element node) and another vector to define the type of elements ( regular or enriched elements). For elements cut by the crack, the element partitioning is used to accurately integrate the discontinuities along the two faces of the element.

The problems presented in this chapter provide an idea about the robustness and validation of the XFEM where less than 2% of error is achieved when appropriate mesh refinement is used. Also it is clear from the problems presented that the structured mesh (quadrilateral elements) provides more accurate results with respect to the unstructured mesh (triangular elements) for the same degrees of freedom and this is because the triangular elements are constant strain elements while the quadrilateral elements are bilinear strain varying elements.

The radius of enrichment $R_{enrich}$ is a very important parameter in XFEM, as increasing its value will increase the final degrees of freedom drastically without any significant improvement in accuracy. The magnitude of the radius of enrichment is basically related to the element edge length $h_e$ and it is recommended to be $1.5h_e \leq R_{enrich} \leq 4.5h_e$.

# CHAPTER FIVE

# DAMAGE TOLERANCE ANALYSIS

## 5.1 Introduction

In this chapter, a brief overview of the safe life design and how the need arises for improving the design methodology to shift the emphasis from crack initiation life to crack propagation life are discussed. Some catastrophic events were reported to show these needs, and the damage tolerance design is defined and its approaches are discussed.

The crack growth for different plates with hole and crack located in different locations and under different types of loading are simulated using XFEM formulation derived in chapter three. Using XFEM, there is no need to re-mesh the domain while the crack grows thus reducing the computational time drastically. Finally, using the concept of damage tolerance analysis, the life of the component is predicted using XFEM.

Many cases studies are investigated in this Chapter including rectangular plate with initial edge crack, plate with hole inside and the crack located in different locations and plate with two holes and the crack emanating from one hole under different types of loading such as tensile, transverse and shear loadings.

## 5.2 Safe-Life Design

In 1954 there were two catastrophic accidents involving the newly developed comet jet airlines. The comet jet was the first jet propelled passenger aircraft in the world to enter into scheduled service. Subsequent investigations and pressure cycle testing of a comet fuselage revealed that the accidents were caused by a structural failure of the

pressure cabin due to metal fatigue cracking [19]. The probable sites of fatigue initiation were identified as fastener holes located in highly stressed regions near the corners of the cabin windows. The comet accidents introduced metal fatigue cracking into the aircraft structural designers' agenda.

As a result, safe-life design was introduced in aircraft engineering following the comet jet accidents. The safe-life approach is based on the number of loading cycles before crack initiation (i.e. failure is assumed when cracks are first formed). The fatigue life was estimated by combining a service stress description with basic fatigue properties obtained from laboratory experiments. The safe life approach is based on the number of loading cycles before crack initiation (mean life). A great deal of uncertainty is associated with the laboratory determination of that quantity. Therefore, the mean life is then divided by a safety factor (from 3-5). The safe-life approach led to several inadequate aircraft design in 1960s [37] such as F-111 (the safe-life for this aircraft was determined to be 4000 flight hours, however one aircraft was lost due to fatigue after only 105 hours), KC-135 (the safe-life for this transport aircraft was determined to be 13000 flight hours, however there were 14 cases of unstable cracking in lower wing skins that occurred between 1800-5000 hours), F-5 (the safe-life design predicted 4000 flight hours, however one of these fighters failed by fatigue cracking in the lower wing skins after 1900 flight hours).

## 5.3 Damage Tolerance Design

To overcome the shortcoming of the safe-life design, damage tolerance design was introduced. The damage tolerance design shifts the emphasis from the crack initiation life to crack propagation life. It is defined as the ability of the structure to resist fracture from

pre-existent cracks for a specified time of period. The initial crack size is usually based on inspection limits and is expected to be a conservative assumption. There are two approaches for the damage tolerance that guarantee that the structure does not fail within the life time: slow crack design, fail-safe design.

The slow crack growth approach is based on selection of the materials and the stress field so that the pre-existent crack will not grow to the critical length during the service time as shown in Figure 5.1. To be more conservative, the prediction time is divided by factor of safety, usually value of 2 is used. Thus, there will be two opportunities to discover the crack before it grows to the critical length.

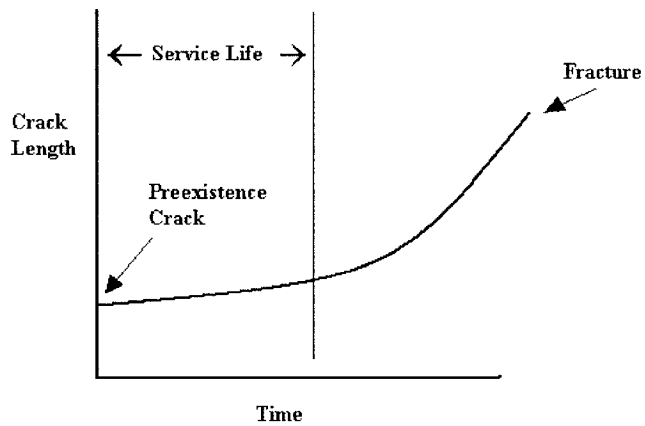


Figure 5.1: Slow crack growth approach

The Fail-Safe approach is based on using multi-load paths, so that failure of single component in the structure does not lead to immediate loss of the whole structure. The load carried by the broken member is immediately picked up by the adjacent structure, and the total fracture is avoided. It is very important for the structure to be repaired since

the extra load carried by the remaining members will shorten their fatigue lives as shown in Figure 5.2.

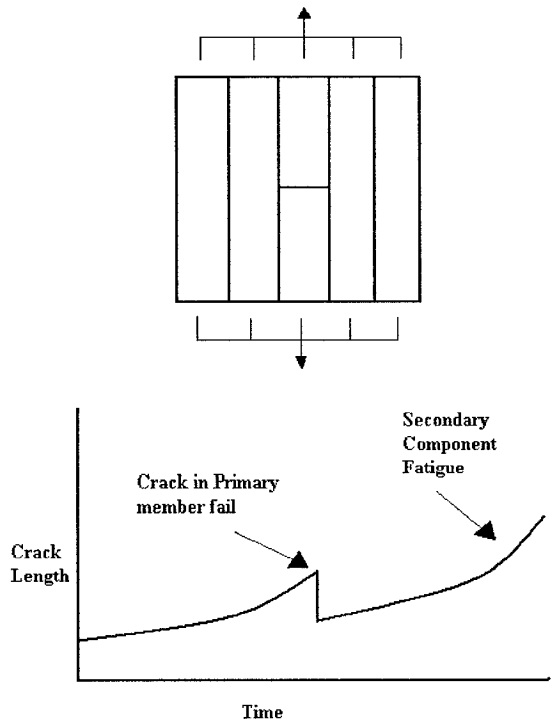


Figure 5.2: Fail safe design

As mentioned in Chapter two, there are many models for the crack growth, one of the most common used is Paris law. It is used to predict the life time for the structure with pre-existence crack to grow to critical length. Fore the sake of clarity, the relative equations are rewritten here as:

$$\frac{da}{dN} = C_p (\Delta K)^{m_p} \tag{5.1}$$

integrating Eq. (5.1) yields:

$$\Delta N = \frac{1}{C_p} \int_{\Delta a} \frac{1}{[\Delta K_e(a)]^{m_p}} da \tag{5.2}$$

which provides explicit equation to evaluate the life time of the structure with pre-existent crack.

## 5.4 Damage Tolerance Analysis using XFEM

As shown in Chapter four, the XFEM has been validated using many problems with cracks located at different locations and less than 2% of error has been obtained where appropriate mesh refinement is used. Considering this, XFEM provides a reliable tool to simulate the crack growth accurately and to predict the life time for different types of structures.

Different types of problems are implemented in this section including initial edge crack growth inside rectangular plate under tensile or shear loading, crack growth in plate with centered crack and inclined crack, crack growth in plate with one crack initiated from a hole and two cracks initiated from a hole. The problems are implemented using the quadrilateral or triangular element mesh and the life time is predicted using the Paris law.

In all problems, plate made of stainless steel with modulus of elasticity $E$ = 190 GPa and Poisson's ratio $\upsilon = 0.305$ is used. The modulus of rigidity for the plate is $G$ = 73.1 GPa and the yield strength is $\sigma_{YS} = 276\ MPa$. The fracture toughness for the stainless steel is $K_{IC} = 66\ MPa\sqrt{m}$ and the stress intensity factor threshold is $K_{th} = 4.6\ MPa\sqrt{m}$. Paris Equation coefficients used are $m_p = 3.6$, $C_p = 4.77\times10^{-11}\ \frac{MN^{-m_p}.m^{1-\frac{m_p}{2}}}{cycle}$. The plane stress condition is also assumed during the simulation of the crack growth in all problems and the LEFM concept is maintained.

In all problems, the crack growth rate $\Delta a$ is considered to be constant. Its value is selected based on the elements edge length $h_e$ used. It is mentioned that the radius of enrichment $R_{enrich}$ is recommended to be limited by $1.5h_e \leq R_{enrich} \leq 4.5h_e$. Here the radius of enrichment used in all problems is selected to be $1.5h_e$. It should be mentioned that having accurate crack growth simulation requires the crack growth rate to be greater than the radius of enrichment ($\Delta a > R_{enrich}$) and this is to represent the tip enrichment functions accurately along the crack segment faces.

### 5.4.1 Plate with initial edge crack at $\beta = 0^o$ under cyclic tensile loading

The plate with dimensions of 10×10 cm and thickness of $t$ = 5 mm has initial crack length of $a$ = 1.8 cm located at the edge of the plate as shown in Figure 5.3. The uniform cyclic loading applied in y-direction results in repeated tensile stress with $\sigma_y^{min} = 0, \sigma_y^{max} = 45\ MPa$.

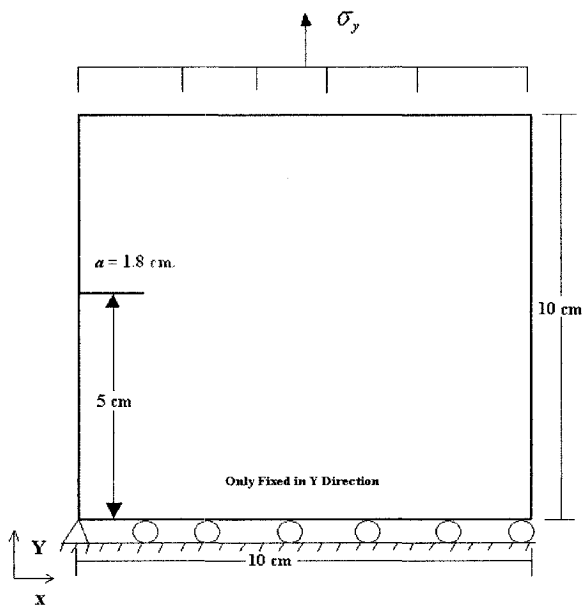


Figure 5.3: Plate with edge crack at $\beta = 0^o$ under uniform tensile loading

The mesh is performed by discretization the domain into $40\times40$ quadrilateral elements (SDOF = 3362). The crack growth is simulated by Paris fatigue law and the maximum principle stress criterion is employed to find its direction. The XFEM technique is used to simulate the crack growth, where no re-meshing is performed during the crack growth simulation and the radius of enrichment is assumed to be $R_{enrich} = 1.5\ h_e$. It is noted that the crack is not necessary to be aligned with the edges of the elements in the mesh.

The crack growth increment is considered for this problem as $\Delta a = 5\ mm$. The analysis shows that the crack will grow in 8 iterations before the equivalent stress intensity factor $K_{Ieq}$ reaches the fracture toughness $K_{IC}$ (see Eq. (2.23)) and resulting in sudden failure. Eq. (5.2) is used to calculate the life time of the plate before the failure occurs and is found to be $5.818\times10^3$ cycles. Figure 5.4 shows the simulation results for the crack path before fracture occurs.

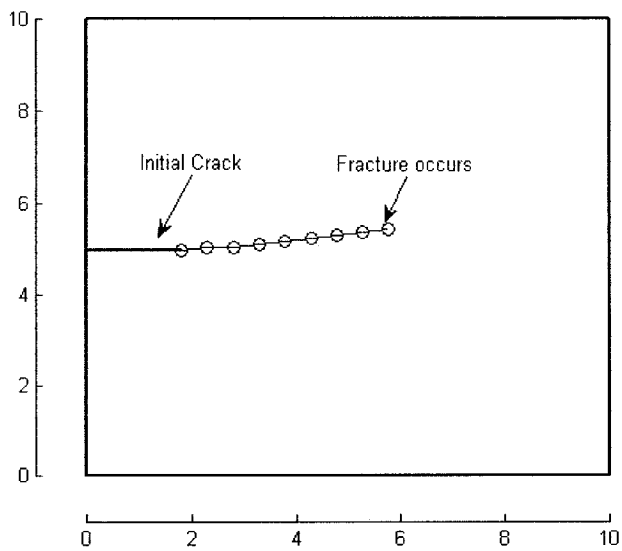


Figure 5.4: Crack growth in plate with edge crack under uniform tensile cyclic loading

Table 5.1 provides $X$ and $Y$ coordinates of the crack tip at each iteration cycle and the estimated first and second modes of the stress intensity factor.

Table 5.1: Tip positions and SIFs for edge crack growth in plate under uniform cyclic tensile loading

| **Iterations** | $X_{tip}$ **cm.** | $Y_{tip}$ **cm.** | $K_I$ $MPa\sqrt{m}$ | $K_{II}$ $MPa\sqrt{m}$ | $K_{Ieq}$ $MPa\sqrt{m}$ | $\frac{r_p}{a}\%$ |
|---|---|---|---|---|---|---|
| **Initial tip location** | 1.8000 | 5.0000 | 16.6328 | -0.5903 | 16.6642 | 3.2233 |
| **1** | 2.2987 | 5.0354 | 18.4832 | 0.2031 | 18.4865 | 3.1044 |
| **2** | 2.7982 | 5.0597 | 22.2207 | -0.6111 | 22.2458 | 3.6927 |
| **3** | 3.2955 | 5.1115 | 27.0538 | -0.2325 | 27.0568 | 4.6349 |
| **4** | 3.7918 | 5.1718 | 32.7616 | -0.1633 | 32.7628 | 5.9017 |
| **5** | 4.2875 | 5.2371 | 39.4320 | -0.2787 | 39.4349 | 7.5561 |
| **6** | 4.7823 | 5.3093 | 47.4573 | 0.0864 | 47.4575 | 9.8033 |
| **7** | 5.2773 | 5.3797 | 58.0689 | 0.1087 | 58.0692 | 13.2928 |
| **Failure** | 5.7726 | 5.4483 | 71.8376 | 0.4984 | 71.8428 | 18.5926 |

As it can be realized, $K_I$ is much larger than $K_{II}$ confirming the fact that mode-*I* is dominant. The value of $K_I$ increases as the length of the crack increases, while the value of $K_{II}$ fluctuates around the zero. This can be referred to the fact that the maximum principle stress criterion assumes that the crack grows in direction perpendicular to the maximum principle stress in the near tip asymptotic field (i.e. the shear is assumed to be zero in this region, and thus mode-*II* does not exist).

The crack grows in path not exactly perpendicular to the tensile loading, this can be explained by the existence of small developed shear and transverse stresses in the crack tip field that affect the direction of the principle stress and as a consequent, affect the crack growth direction.

The last column in Table 5.1 represents the ratio between the radius of the crack tip plastic zone $r_p$ and the crack length $a$. As it can be realized, this ratio is almost less than 10% for all crack growth iterations. This confirm the applicability of the LEFM concept.

### 5.4.2 Plate with initial edge crack at $\beta = 0^o$ under cyclic shear loading

In this problem, the plate dimensions, thickness, initial crack length and orientation are similar to problem in Section 5.4.1 except that the plate is under shear cyclic loading in which $\tau_{xy}^{\min} = 0, \tau_{xy}^{\max} = 20\ MPa$ as shown in Figure 5.5

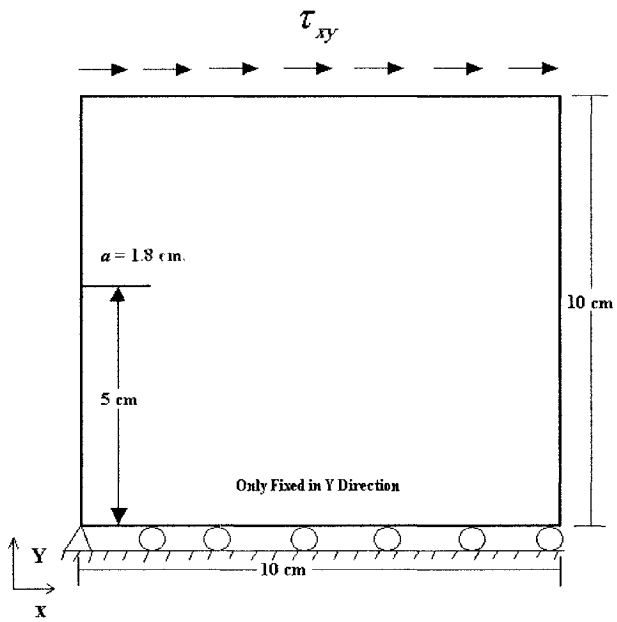


Figure 5.5: Plate with edge crack under cyclic shear loading

Same discretization model is performed in this problem as that in previous problem. Constant crack growth rate of $\Delta a = 5\ mm$ is also assumed with same radius of enrichment. The analysis using XFEM shows that the crack will grow in 9 iterations before the equivalent stress intensity factor $K_{Ieq}$ reaches the fracture toughness $K_{IC}$

resulting sudden failure. Figure 5.6 shows the crack path during the load cycling. It is noted the crack bends down from its initial direction in a certain angle confirming the mixed-mode effect in the crack tip field. Thus the magnitudes of $\sigma_x, \sigma_y$ and $\tau_{xy}$ will affect the magnitude and the direction of the principle stresses and as a consequent, the direction of the crack growth.

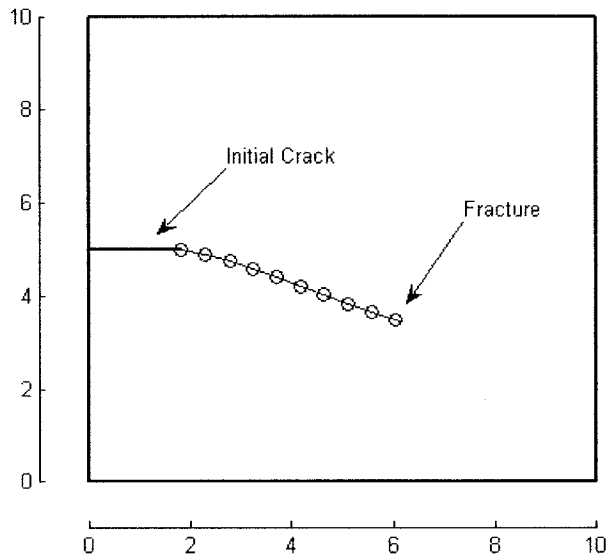


Figure 5.6: Crack growth in plate with edge crack under uniform shear cyclic loading

Table 5.2 provides $X$ and $Y$ coordinates for the crack tip at each iteration cycle and the estimated first and second modes of the stress intensity factor. It is interesting to note that even for this case mode-$I$ is the dominant deformation mode at the initial tip before the crack grows, this leads to the fact that the dominant stress in the near tip asymptotic fields is the tensile stress. Similar to the previous example the value of $K_{II}$ is insignificant compared with $K_I$ during iteration cycles due to applying the maximum principle stress

criterion. The life estimation time of the plate in term of number of cycles is found to be $7.271\times10^{3}$.

Table 5.2: Tip positions and SIFs for edge crack growth in plate under shear cyclic loading

| Iterations | $X_{tip}$ cm. | $Y_{tip}$ cm. | $K_I$ $MPa\sqrt{m}$ | $K_{II}$ $MPa\sqrt{m}$ | $K_{Ieq}$ $MPa\sqrt{m}$ |
|---|---|---|---|---|---|
| **Initial tip location** | 1.8000 | 5.0000 | 16.1042 | 2.0089 | 16.4704 |
| **1** | 2.2855 | 4.8807 | 17.8777 | 0.2312 | 17.8822 |
| **2** | 2.7679 | 4.7488 | 21.1749 | 0.8206 | 21.2225 |
| **3** | 3.2385 | 4.5801 | 24.9785 | 0.2115 | 24.9812 |
| **4** | 3.7063 | 4.4035 | 28.9795 | 0.3064 | 28.9844 |
| **5** | 4.1702 | 4.2171 | 33.6236 | 0.1597 | 33.6247 |
| **6** | 4.6324 | 4.0262 | 39.2967 | -0.1347 | 39.2974 |
| **7** | 5.0958 | 3.8385 | 46.2433 | -0.2364 | 46.2451 |
| **8** | 5.5611 | 3.6556 | 55.1588 | -0.4666 | 55.1647 |
| **Failure** | 6.0295 | 3.4805 | 66.5373 | -0.6768 | 66.5476 |

### 5.4.3 Plate with initial edge crack inclined at angle $\beta = 15^{o}$ under cyclic tensile loading

The same plate discussed in section 5.4.1 is studied again. However in this plate the initial crack is inclined at angle $\beta = 15^{o}$. The plate is under cyclic tensile loading with $\sigma_y^{\min} = 0, \sigma_y^{\max} = 45\ MPa$ as shown in Figure 5.7.

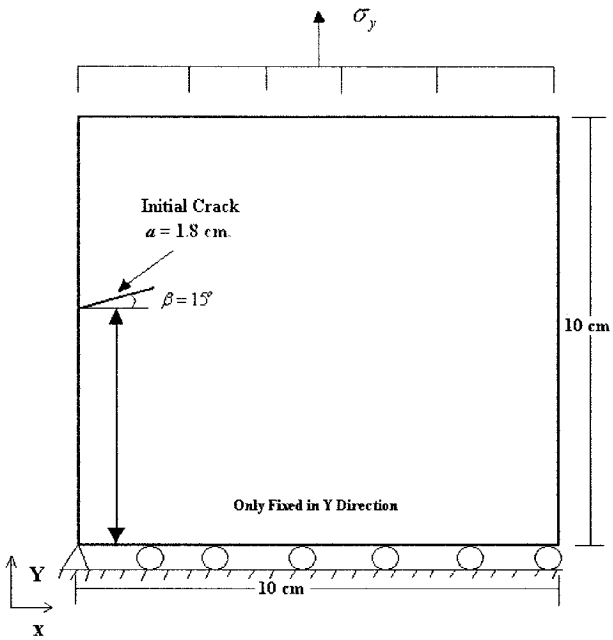


Figure 5.7: Plate with edge crack inclined at $\beta = 15^o$

The plate is discretized with $40 \times 40$ quadrilateral elements resulting in SDOF = 3362. The crack growth rate is assumed to be $\Delta a = 5\ mm$ . The analysis results using XFEM shows that the crack will grow in 8 iterations before the equivalent stress intensity factor $K_{Ieq}$ reaches the fracture toughness $K_{IC}$. The life of the plate in term of number of loading cycles is found to be $5.815 \times 10^3$ cycles. Figure 5.8 shows the crack path during the load cycling up to the fracture point.

Table 5.3 provides $X$ and $Y$ coordinates for the crack tip at each iteration and the estimated first and second modes of the stress intensity factor.

It is noted that $K_{II}$ in the initial location of the crack tip is considerable due to initial angle of $\beta = 15^o$ . Once the crack starts growing, the $K_{II}$ reduces to very small value (close to zero) due to applying the maximum principle stress criterion

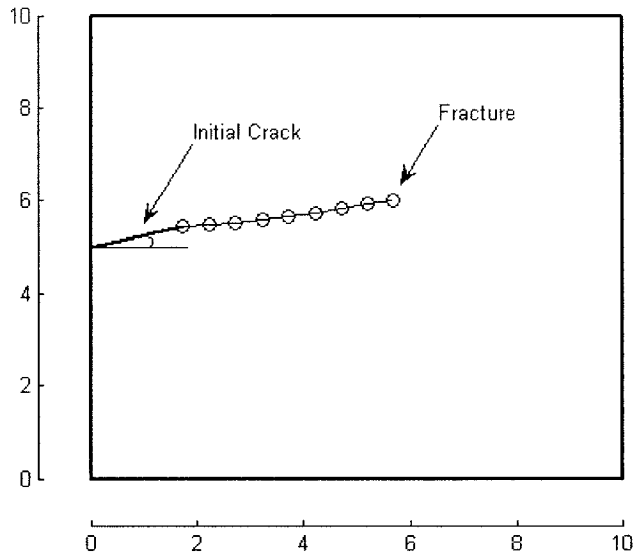


Figure 5.8: Crack growth in plate with initial edge crack inclined at $\beta = 15^{o}$ under uniform tensile cyclic loading

Table 5.3: Tip positions and SIFs for crack growth in plate with initial inclined edge crack

| **Iterations** | $X_{tip}$ **cm.** | $Y_{tip}$ **cm.** | $K_I$ $MPa\sqrt{m}$ | $K_{II}$ $MPa\sqrt{m}$ | $K_{Ieq}$ $MPa\sqrt{m}$ |
|---|---|---|---|---|---|
| **Initial tip location** | 1.7387 | 5.4659 | 14.2699 | 1.8052 | 14.6034 |
| **1** | 2.2386 | 5.4747 | 18.3006 | -0.8224 | 18.3558 |
| **2** | 2.7357 | 5.5281 | 22.3946 | -0.0236 | 22.3946 |
| **3** | 3.2327 | 5.5826 | 27.3350 | -0.4320 | 27.3452 |
| **4** | 3.7278 | 5.6528 | 33.1337 | -0.4201 | 33.1417 |
| **5** | 4.2209 | 5.7355 | 39.7253 | -0.4503 | 39.7330 |
| **6** | 4.7120 | 5.8293 | 47.8679 | -0.2100 | 47.8693 |
| **7** | 5.2023 | 5.9275 | 58.3431 | 0.1420 | 58.3436 |
| **Failure** | 5.6930 | 6.0233 | 71.9713 | 0.1283 | 71.9716 |

### 5.4.4 Plate with initial central crack at $\beta = 0^o$ under uniform cyclic tensile loading

In this problem, the plate has similar dimensions and thickness as the previous problems with a central crack length of $2a$ = 1.5 cm. The plate is again under uniform tensile cyclic loading with $\sigma_y^{min} = 0, \sigma_y^{max} = 100\ MPa$ as shown in Figure 5.9.

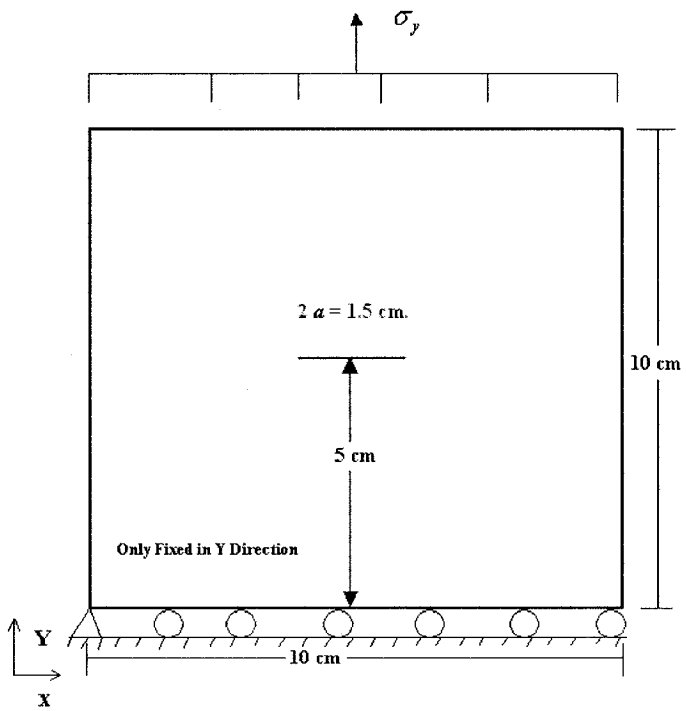


Figure 5.9: Plate with central crack at $\beta = 0^o$

The domain is discretized using triangular elements with element edge length $h_e$ = 2 mm. The Background mesh degrees of freedom is 3816 and the crack growth increment is again assumed to be $\Delta a = 5\ mm$ with radius of enrichment $R_{enrich}$ = 4.5 mm. The crack growth simulation is accomplished for 7 iterations as shown in Figure 5.10 before the

equivalent stress intensity factor $K_{Ieq}$ reaches the fracture toughness $K_{IC}$ and results in sudden failure.

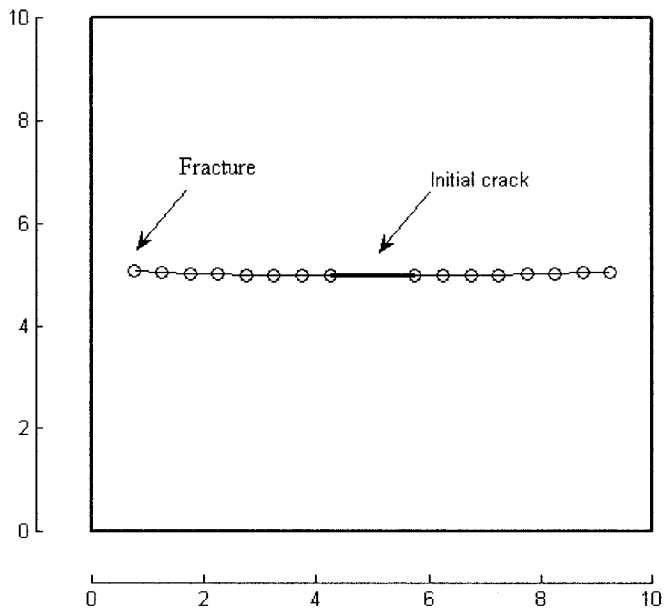


Figure 5.10: Crack growth in plate with initial central crack at $\beta = 0^o$

The tip 1 and tip 2 coordinates and the first and second modes of the stress intensity factor at each iteration are provided in Table 5.4. It can be seen that $K_{II}$ fluctuates around zero causing the kinking nature for the crack growth. The life time is predicted using Paris law to be $3.812 \times 10^3$.

Table 5.4: Tip positions and SIFs for crack growth in plate with initial central crack

| Iterations | $X_{tip1}$ cm. | $Y_{tip1}$ cm. | $X_{tip2}$ cm. | $Y_{tip2}$ cm. | $K_I$ $MPa\sqrt{m}$ | $K_{II}$ $MPa\sqrt{m}$ | $K_{Ieq}$ $MPa\sqrt{m}$ |
|---|---|---|---|---|---|---|---|
| **Initial tip location** | 4.2500 | 5.0000 | 5.7500 | 5.0000 | 15.0900 | -0.0880 | 15.0908 |
| **1** | 3.7500 | 4.9942 | 6.2500 | 4.9941 | 20.3700 | 0.1960 | 20.3728 |
| **2** | 3.2500 | 4.9979 | 6.7500 | 4.9979 | 25.2600 | -0.0250 | 25.2600 |
| **3** | 2.7501 | 5.0007 | 7.2499 | 5.0006 | 31.0100 | 0.4360 | 31.0192 |
| **4** | 2.2503 | 5.0175 | 7.7497 | 5.0173 | 37.3000 | 0.1570 | 37.3010 |
| **5** | 1.7508 | 5.0385 | 8.2492 | 5.0383 | 46.3700 | -0.3390 | 46.3737 |
| **6** | 1.2510 | 5.0522 | 8.7490 | 5.0521 | 59.1100 | 0.4920 | 59.1161 |
| **Failure** | 0.7515 | 5.0743 | 9.2486 | 5.0740 | 77.7600 | -1.0870 | 77.7828 |

### 5.4.5 Plate with initial central crack at $\beta = 45^o$ under uniform cyclic tensile loading

In this problem similar plate dimensions and thickness are used with initial crack of length $2a$ = 1.5 cm located at the center of the plate and inclined at $\beta = 45^o$. The plate is under uniform tensile cyclic loading with $\sigma_y^{\min} = 0, \sigma_y^{\max} = 100\ MPa$ as shown in Figure 5.11.

The discretized model, crack growth rate and radius of enrichment are similar to that of previous section. The XFEM simulation expects the failure after 7 iterations where the fracture toughness is reached to the equivalent stress intensity factor. The crack growth path is shown in Figure 5.12.

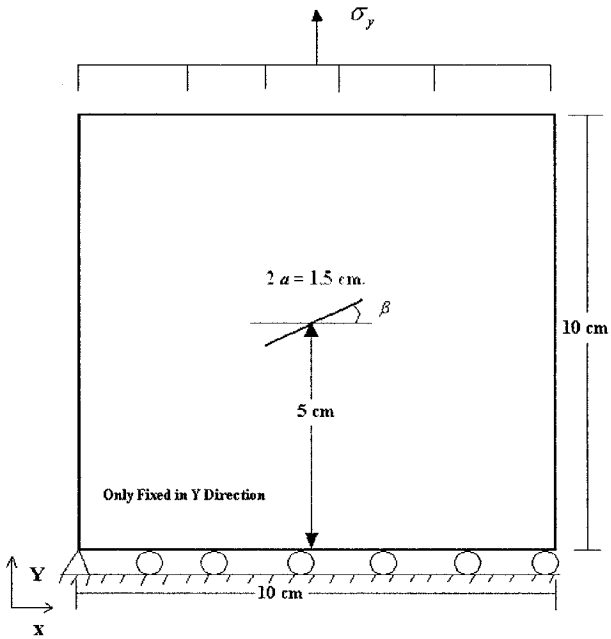


Figure 5.11: Plate with central crack inclined at $\beta = 45^o$

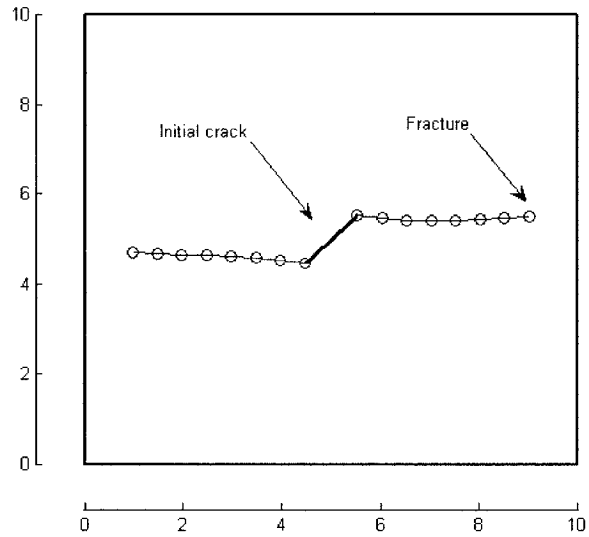


Figure 5.12: Crack growth in plate with initial central crack at $\beta = 45^o$ (units in cm)

The tip1 and tip 2 coordinates and the first and second modes of the stress intensity factor are provided in Table 5.5. The life time for the plate with the central crack inclined at $\beta = 45^o$ is found to be $7.545 \times 10^3$ cycles.

Table 5.5: Tip positions and SIFs for crack growth in plate with inclined central crack

| Iterations | $X_{tip1}$ cm. | $Y_{tip1}$ cm. | $X_{tip2}$ cm. | $Y_{tip2}$ cm. | $K_I$ $MPa\sqrt{m}$ | $K_{II}$ $MPa\sqrt{m}$ | $K_{Ieq}$ $MPa\sqrt{m}$ |
|---|---|---|---|---|---|---|---|
| **Initial tip location** | 4.4697 | 4.4697 | 5.5303 | 5.5303 | 7.9132 | 7.6568 | 13.8787 |
| **1** | 3.9741 | 4.5360 | 6.0262 | 5.4663 | 15.6541 | -0.3699 | 15.6631 |
| **2** | 3.4759 | 4.5789 | 6.5248 | 5.4282 | 23.3668 | -0.351 | 23.3679 |
| **3** | 2.9767 | 4.6067 | 7.0244 | 5.4093 | 29.4247 | -0.118 | 29.4207 |
| **4** | 2.4773 | 4.6306 | 7.5242 | 5.4226 | 34.6233 | 0.0235 | 34.6200 |
| **5** | 1.9779 | 4.6552 | 8.0238 | 5.4426 | 43.3120 | -0.1639 | 43.3109 |
| **6** | 1.4783 | 4.6760 | 8.5234 | 5.4632 | 54.0311 | 0.8539 | 54.0502 |
| **Failure** | 0.9797 | 4.7125 | 9.0223 | 5.4967 | 67.3281 | -1.1675 | 67.3504 |

At the initial crack tips the exact first and second modes of the stress intensity factor are $K_I = K_{II} = 7.675\ MPa$ which are in good agreement with the results in the first row of the Table 5.5 obtained by XFEM. The small difference between the exact solution and the solution obtained using XFEM for the mode-*I* stress intensity factor can be minimized by increasing the tip radius of enrichment. It is noted that when the crack starts growing the value of $K_{II}$ is reduced to very small values compared to $K_I$ confirming the dominant of mode-*I* during the crack growth.

### 5.4.6 Plate with central hole and two emanating cracks

In this problem, hole with radius of $R$ = 1 cm is located in the center of plate which has the dimensions of 10×10 cm and thickness of $t$ = 5 mm. The hole has two cracks emanating from its circumference with $a$ = 1.5 cm as shown in Figure 5.13. The plate is under uniform tensile loading with $\sigma_y^{\min} = 0, \sigma_y^{\max} = 100\ MPa$

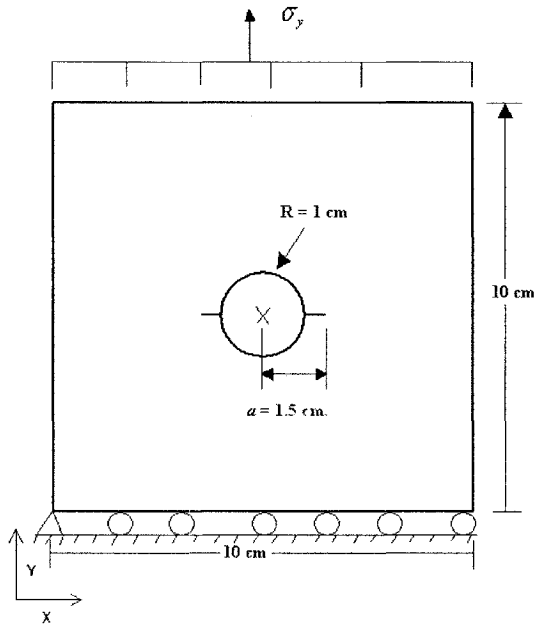


Figure 5.13: Plate with central hole and two emanating cracks

The domain discretization, radius of enrichment and crack growth rate are similar to the previous section where the triangular elements are used in the background mesh with total degrees of freedom of 3816. The XFEM is used to model the crack growth where the analysis shows that the crack will grow in 5 iterations before the failure occurs. Figure 5.14 shows the path of the crack growth from its initial up to fracture point.

The tip locations for crack 1 and 2 and the first and second modes of the stress intensity factors are provided in Table 5.6. The life time is predicted as 934 cycles before the fracture occurs.

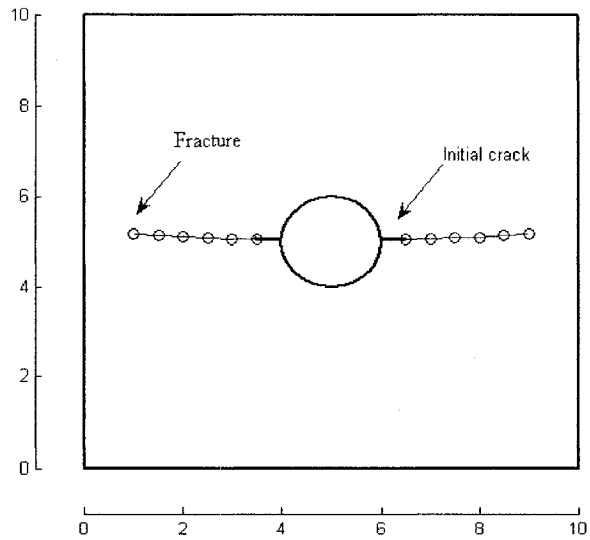


Figure 5.14: Crack growth in plate with central hole and two emanating cracks

(units in cm)

Table 5.6: Tip positions and SIFs for cracks 1 and 2 growth in plate with centered hole

| **Iterations** | $X1_{tip}$ **cm.** | $Y1_{tip}$ **cm.** | $X2_{tip}$ **cm.** | $Y2_{tip}$ **cm.** | $K_I$ $MPa\sqrt{m}$ | $K_{II}$ $MPa\sqrt{m}$ | $K_{Ieq}$ $MPa\sqrt{m}$ |
|---|---|---|---|---|---|---|---|
| **Initial tip location** | 3.5000 | 5.0500 | 6.5000 | 5.0500 | 25.2752 | 0.0101 | 25.2752 |
| **1** | 3.0001 | 5.0601 | 6.9999 | 5.0603 | 30.1255 | 0.0288 | 30.1255 |
| **2** | 2.5012 | 5.0932 | 7.4994 | 5.0828 | 37.2457 | -0.0287 | 37.2457 |
| **3** | 2.0014 | 5.1073 | 7.9990 | 5.1017 | 45.3251 | 0.0563 | 45.3252 |
| **4** | 1.5034 | 5.1522 | 8.4973 | 5.1430 | 53.4452 | -0.0245 | 53.4452 |
| **Failure** | 1.0045 | 5.1858 | 8.9964 | 5.1733 | 66.6654 | 0.0827 | 66.6656 |

Examination of Table 5.6 reveals that the values of $K_I$ and $K_{II}$ in the initial crack location show mode-*I* is the dominant mode which cause the crack to grow horizontally. It is noted that $K_I$ increases as the crack length increases while $K_{II}$ fluctuates around zero.

### 5.4.7 Plate with two holes and single crack emanating from the left hole subjected to tensile cyclic loading

The plate has dimensions of 10×10 cm and thickness of $t$ = 5mm is used in this problem. The plate has two holes with radius of $R$ = 1.25 cm. The center of the holes is located 2.5 cm away from the edges of the plate. One crack is initiated from left hole with initial length of $a$ = 5 mm, and inclined at angle of $\beta = 15^{o}$ as shown in Figure 5.15. The plate is also under uniform cyclic tensile loading with $\sigma_y^{\min} = 0, \sigma_y^{\max} = 45\ MPa$.

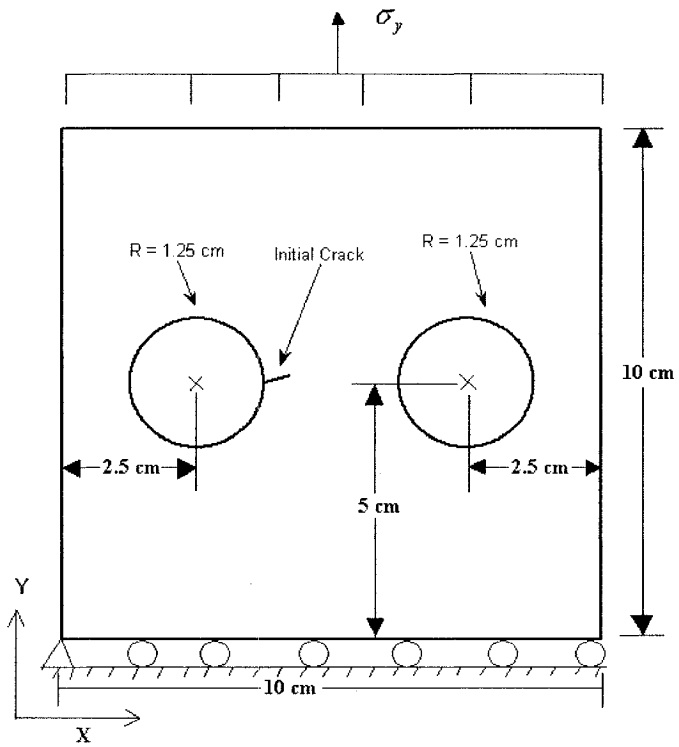


Figure 5.15: Plate with two holes and single crack emanating from the left hole subjected to tensile cyclic loading

The domain is discretized using triangular element mesh with variable density as shown in Figure 5.16. The crack growth increment is set to $\Delta a = 3.5\ mm$ . The growth is simulated for 5 iterations where the crack reaches the right hole, and the prediction time is found to be $9.348 \times 10^4$. Figure 5.17 shows the crack growth path. As shown, the crack grows from its initial location and continues to the second hole in the plate.

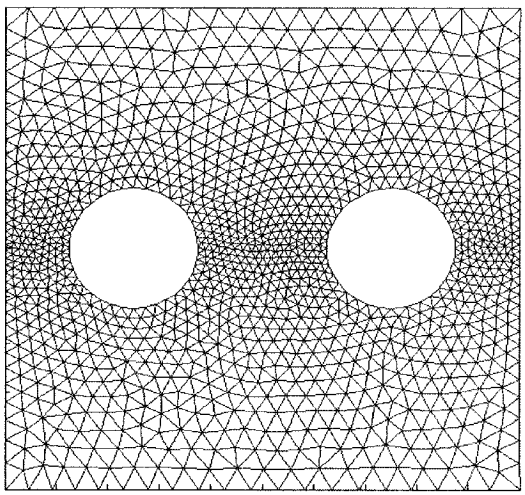

Figure 5.16: Domain discretization of plate with two holes

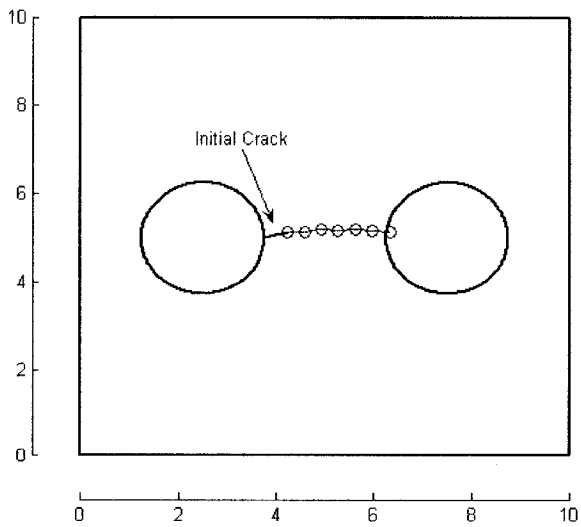


Figure 5.17: Crack growth path in plate with two holes and crack emanating from the left hole (units in cm)

Table 5.7 provides $X$ and $Y$ coordinates of the crack tip at each iteration and the estimated first and second modes of the stress intensity factor.

Table 5.7: Tip positions and SIFs for crack growth in plate with two holes and single crack emanating from the left hole

| **Iterations** | $X_{tip}$ **cm.** | $Y_{tip}$ **cm.** | $K_I$ $MPa\sqrt{m}$ | $K_{II}$ $MPa\sqrt{m}$ | $K_{Ieq}$ $MPa\sqrt{m}$ |
|---|---|---|---|---|---|
| **Initial tip location** | 4.2325 | 5.1294 | 13.5729 | 2.0530 | 13.6496 |
| **1** | 4.5823 | 5.1203 | 8.0995 | -0.7454 | 8.1988 |
| **2** | 4.9282 | 5.1742 | 8.3508 | 0.9174 | 8.4213 |
| **3** | 5.2776 | 5.1534 | 10.2602 | -0.6060 | 10.2998 |
| **4** | 5.6270 | 5.1737 | 24.3257 | 0.8719 | 24.3418 |
| **5** | 5.9769 | 5.1689 | 15.0849 | 0.7055 | 15.1332 |

The $K_{II}$ has considerable value at the initial crack before it grows; this is because the crack is initially inclined at angle $\beta = 15^{o}$. The analysis shows that the crack initiated from the first hole under the uniform tensile loading reaches the circumference of the second hole.

## 5.5 Conclusion

The damage tolerance design is more conservative than the safe-life design. It deals with predicting the life time for a structure with pre-existent crack to grow to the critical length. This shifts the concepts for designers from the crack initiation life to the crack propagation life. Using the Paris law, it is possible to predict the life time for the

structures, provided that the stress intensity factors are known and the crack path is known during the growth of the crack from its initial length to the critical length.

The full analysis and simulation of the crack growth can be accomplished accurately and efficiently using the XFEM, where no re-meshing is required each time the crack grows and there is no need for the crack to be aligned with the elements edges in the mesh.

Through numerous illustrative examples, it has been shown that XFEM can be used in damage tolerance applications to predict the life of the components accurately and efficiently.

# CHAPTER SIX

# CONCLUSIONS AND FUTURE WORK

## 6.1 Summary

The regular FEM is not well-suited for geometries with evolving discontinuities since there is a need for re-meshing each time the discontinuity evolves. Besides the need for high mesh density in the crack tip region due to the singularities, regular FEM requires re-meshing when the crack grows thus increasing the computational time drastically. Different from the regular finite element where the crack is modeled explicitly by aligning the crack faces with the edges of the elements in the mesh, the crack in XFEM can be modeled implicitly in the mesh, thus no re-meshing is required each time the crack grows.

The crack modeling using XFEM is discussed and implemented by selecting the nodes beside the crack to be enriched by the discontinuity and the tip enrichment functions. The nodes selection is performed through special enrichment scheme.

The XFEM formulation is presented and it is concluded that the XFEM is the natural extension of the regular finite element as it combines the regular degrees of freedom resulted from FEM and the extra degrees of freedom obtained from the enrichment functions. Thus the XFEM can be joined easily with the finite element packages to account for the discontinuities.

The XFEM implementation procedure is explained starting from discretizing the domain and obtaining the global stiffness matrix. This has been done using regular finite element mesh generator. The procedure continued until obtaining the nodal

displacements, the elements stresses and the stress intensity factors in mixed-mode problems. This has been conducted through comprehensive investigation on the XFEM. A formulation that creates the enriched approximation from the interaction of crack geometry with the background mesh is derived. This allows the entire crack to be treated independently without addressing the mesh.

As mentioned in XFEM, the extra degrees of freedom are resulted from the enrichment functions. Two types of enrichment functions are used in the technique. The first function accounts for the discontinuities along the crack faces and far from the crack tip, two degrees of freedom for 2D domain will be added to the global degrees of freedom for each node selected to be enriched by this function. The second function is the tip enrichment function, where eight degrees of freedom for 2D domain will be added to the global degrees of freedom for each node selected to be enriched by the tip enrichment functions.

Different examples are studied to show the XFEM validation and robustness. This is accomplished by comparing the stress intensity factors resulted using XFEM with the exact solutions. It has been demonstrated that the structural mesh (quadrilateral elements) provides more accurate results than the unstructured mesh (triangular elements) and even for course mesh the results obtained can be considered as acceptable results when comparing with the exact solutions.

The importance of the radius of enrichment and its effect on the accuracy of the XFEM especially for course mesh and on the final degrees of freedom are discussed. It is shown that the radius of enrichment should not be less than $1.5h_e$ to ensure that at least one layer of elements bear the exact XFEM solution. It is also shown that when the radius

of enrichment increases the accuracy of the XFEM solution increases. Thus it is recommended that the radius of enrichment does not exceed a certain limit.

The crack growth is simulated using XFEM for plate with different cracks located at the edges, the center or initiated from holes located in the plate. It is shown that the crack growth takes place regardless of the discretized domain and the locations of the nodes and elements in the background mesh. It has been shown that the XFEM is a reliable tool to predict the service-life for the cracked structures, since no re-meshing is required.

Finally, the potential application of XFEM in damage tolerance analysis has been demonstrated.

## 6.2 Future Work

To simplify the enrichment scheme, more advanced and efficient searching algorithms should be established in the XFEM code to find the nodes that are required to be enriched quickly and easily.

Using the higher order elements is still in its early stages and more work is required to investigate its efficiency. This can be accomplished by using the higher order elements in the background mesh instead of the quadrilateral or the triangular elements. Also the enrichment scheme can be performed by selecting all the nodes that their supports are cut by the crack and should be enriched by the enrichment functions.

The enrichment geometry is selected as a circle with the center at the crack tip. More investigations are required to obtain more efficient geometries that give more accurate results with less extra degrees of freedom. The predictable shape of the plastic zone developed around the crack tip for both plane stress and plane strain conditions can be good start for such investigations.

XFEM is basically designed to model cracks. More efforts are still needed to expand the technique into different engineering fields such as civil engineering structures, automobile, heat transformation and the biomedical engineering.

Modeling holes and inclusions is also possible using the XFEM by developing new enrichment function and considering special enrichment scheme for the nodes that their supports are cut by the inclusion geometry.

# REFRENCES


[1] Belytschko, T. Lu, Y. and Gu, L. "Element-free galerkin methods". International Journal for Numerical Methods in Engineering 1994;37:229-256.

[2] Belytschko, T. and Black, T. "Elastic crack growth in finite elements with minimal remeshing". International Journal for Numerical Methods in Engineering 1999; 45(5):601-620.

[3] Fleming, M., Chu, Y. A., Moran, B. and Belytschko, T. "Enriched element-free galerkin methods for singular fields". Journal for Numerical Methods in Engineering 1997; 40: 1483-1504.

[4] Melenk, J. M. and Babuska, I. " The partition of unity finite element method: basic theory and applications". Computer Methods in Applied Mechanics and Engineering 1996;139:289-314.

[5] Melenk, J. M. and Babuska, I. " Partition of unity method". International Journal for Numerical Methods in Engineering 1997;40:727-758.

[6] Moes, N., Dolbow, J. and Belytschko, T. "A finite element method for crack growth without remeshing". International Journal for Numerical Methods in Engineering 1999; 46: 131-150.

[7] Sukumar, N, and Prevost, J. H. "Modeling quasi-static crack growth with the extended finite element method Part I: Computer implementation". International

[8] Sukumar, N., Huang, R. and Prevost, J. H. "Modeling quasi-static crack growth with the extended finite element method Part II: Numerical applications". International Journal of Solids and Structure 2003;40:7539-7552.

[9] Bechet, E., Minnebo, H., Moes, N. and Burgardt, B. " Improved implementation and

robustness study of the X-FEM for stress analysis around cracks". International Journal for Numerical Methods in Engineering 2005;64:1033-1056.

[10] Bellec, J. and Dolbow, J. "A note on enrichment functions for modeling crack nucleation".2003

[11] Sukumar, N., Srolovitz, D., Baker, T. and Prevost, J. "Brittle fracture in polycrystalline microstructures with the extended finite element method". International Journal for Numerical Methods in Engineering 2003;56(14):2015-2037.

[12] Daux, C., Moes, N., Dolbow, J. and Sukumar, N. "Arbitrary branched and intersecting cracks with the extended finite element method". International Journal for Numerical Methods in Engineering 2000;48:1741-1760.

[13] Sukumar, N., Moes, N., Moran, B. and Belytschko, T. "Extended finite element method for three-dimensional crack modeling". International Journal for Numerical Methods in Engineering 2000;48:1549-1570.

[14] Moes, N., Gravouil, A. and Belytschko, T. "Non-planar 3d crack growth by the extended finite element method and level sets. part I: Mechanical model". International Journal for Numerical Methods in Engineering 2002; 53:2549-2568.

[15] Sukumar, N., Chopp, D. and Moran, B. "Extended finite element method and fast marching method for three dimensional fatigue crack propagation". Engineering Fracture Mechanics 2003;70:29–48.

[16] Rook, D. P., Baratta, F. I. and Cartwright D. J. "Simple methods of determining stress intensity factors". Engineering Fracture Mechanics 1977;9:189-210.

[17] Cruse, A. "Numerical evaluation of elastic stress intensity factors by the boundary-

integral equation method". The surface crack: physical problems and computational solutions, Swedlow L. J. (ED), pp. 153-170, ASME, New York 1972.

[18] Synder, D. and Cruse, A. "Boundary-integral equation analysis of cracked anisotropic plates". International Journal of Fracture 1975;11:315-328.

[19] Salgado, N. "Boundary element methods for damage tolerance design of aircraft structures". Computational Mechanics Publication, Britain 1998.

[20] Perez, N. "Fracture Mechanics". Kluwer Academic Publisher, Boston 2004.

[21] Paris, P. C. and Erdogan, F. "A critical analysis of crack propagation laws". Journal of Basis Engineering, Trans. ASME 1963;85: 528-534.

[22] Forman, R., Kearney, V. and Engle, R. "Numerical analysis of crack propagation in cyclic-loaded structures". Journal of Basic Engineering 1967;89:459-464.

[23] Walker, K. "The effect of stress ratio during crack propagation and fatigue for 2024-T3 and 7075-T6 Aluminium". ASTM 1970;STP 462.

[24] Tanaka, K. "Fatigue crack propagation from a crack inclined to the cyclic tensile axis". Engineering Fracture Mechanics 1974;6:493-507.

[25] Nuismer, R. "An energy release rate criterion for mixed-mode fracture". International Journal of Fracture 1975;11:245-250.

[26] Sih, G. "Energy-density concept in fracture mechanics". Engineering Fracture Mechanics 1973;5:1037-1040.

[27] Erdogan, F. and Sih, G. "On the crack extension in plate under plane loading and transverse shear". Journal of Basic Engineering 1963;85:519-527.

[28] Yau, J., Wang, S. and Corten H. "A mixed-mode crack analysis of isotropic solids

using conservation law of elasticity". Journal of applied mechanics 1980; 47:335-341.

[29] Shish, C. and Asaro, R. "Elastic-plastic analysis of cracks on biomaterial interfaces: part I-small scale yielding". Journal of applied mechanics 1988;55:299-316.

[30] Moran, B. and Shih, F. "Crack tip and associated domain integrals from momentum and energy balance". Engineering Fracture Mechanics 1987;27:615-642.

[31] Nikishkov, G. P. and Atluri, S. N. "Calculation of fracture mechanics parameters for an arbitrary 3-dimensional crack by the equivalent domain integral method". International Journal for Numerical Methods in Engineering 1987;24:1801-1821.

[32] Broek, D. "Elementary engineering fracture mechanics". Martinus Nijhoff Publishers, Netherlands 1984.

[33] Parker, A. P. "The mechanics of fracture and fatigue". E. & F. N. spon, London, 1981.

[34] Brown, W., Srawley, J. E. and Srawley J. R. "Plane strain crack toughness testing of high strength metallic materials". ASTM STP 410,1966.

[35] Koiter, W. "Note on the stress intensity factor for sheet strips with cracks under tensile load". University of Technology, Report No. 314, Delft, Netherlands 1965.

[36] Rooke, D. P. and Cartwright D.J., "Compendium of stress intensity factors". Her majesty's stationary office, England, 1976.

[37] Alten, F. and Grandt JR. "Fundamentals of structural integrity". John Wiley and Sons Inc. New Jersey 2004.

# APPENDIX A

$$I^{(1,2)} = \int_A \left[ \sigma_{ij}^{(1)} \frac{\partial z_i^{(2)}}{\partial \chi_1} + \sigma_{ij}^{(2)} \frac{\partial z_i^{(1)}}{\partial \chi_1} - W^{(1,2)} \delta_{1j} \right] \frac{\partial q}{\partial \chi_j} dA \tag{A.1}$$

$$W^{(1,2)} = \frac{1}{2}\left[ \sigma_{ij}^{(1)} \varepsilon_{ij}^{(2)} + \sigma_{ij}^{(2)} \varepsilon_{ij}^{(1)} \right] = \sigma_{ij}^{(1)} \varepsilon_{ij}^{(2)} = \sigma_{ij}^{(2)} \varepsilon_{ij}^{(1)}$$

Expanding each term in equation (A.1) give

$$\sigma_{ij}^{(1)} \frac{\partial z_i^{(2)}}{\partial \chi_1} \frac{\partial q}{\partial \chi_j} = \sigma_{11}^{(1)} \frac{\partial z_1^{(2)}}{\partial \chi_1} \frac{\partial q}{\partial \chi_1} + \sigma_{12}^{(1)} \frac{\partial z_1^{(2)}}{\partial \chi_1} \frac{\partial q}{\partial \chi_2} + \sigma_{21}^{(1)} \frac{\partial z_2^{(2)}}{\partial \chi_1} \frac{\partial q}{\partial \chi_1} + \sigma_{22}^{(1)} \frac{\partial z_2^{(2)}}{\partial \chi_1} \frac{\partial q}{\partial \chi_2} \tag{A.2}$$

$$\sigma_{ij}^{(2)} \frac{\partial z_i^{(1)}}{\partial \chi_1} \frac{\partial q}{\partial \chi_j} = \sigma_{11}^{(2)} \frac{\partial z_1^{(1)}}{\partial \chi_1} \frac{\partial q}{\partial \chi_1} + \sigma_{12}^{(2)} \frac{\partial z_1^{(1)}}{\partial \chi_1} \frac{\partial q}{\partial \chi_2} + \sigma_{21}^{(2)} \frac{\partial z_2^{(1)}}{\partial \chi_1} \frac{\partial q}{\partial \chi_1} + \sigma_{22}^{(2)} \frac{\partial z_2^{(1)}}{\partial \chi_1} \frac{\partial q}{\partial \chi_2} \tag{A.3}$$

$$W^{(1,2)} \delta_{1j} \frac{\partial q}{\partial \chi_j} = \left[ \sigma_{11}^{(2)} \frac{\partial z_1^{(1)}}{\partial \chi_1} + \sigma_{12}^{(2)} \left( \frac{\partial z_1^{(1)}}{\partial \chi_2} + \frac{\partial z_2^{(1)}}{\partial \chi_1} \right) + \sigma_{22}^{(2)} \frac{\partial z_2^{(1)}}{\partial \chi_2} \right] \frac{\partial q}{\partial \chi_1} \tag{A.4}$$

Then

$$\begin{aligned} I^{(1,2)} = & \int_A \left[ \sigma_{11}^{(1)} \frac{\partial z_1^{(2)}}{\partial \chi_1} \frac{\partial q}{\partial \chi_1} + \sigma_{12}^{(1)} \frac{\partial z_1^{(2)}}{\partial \chi_1} \frac{\partial q}{\partial \chi_2} + \sigma_{21}^{(1)} \frac{\partial z_2^{(2)}}{\partial \chi_1} \frac{\partial q}{\partial \chi_1} + \sigma_{22}^{(1)} \frac{\partial z_2^{(2)}}{\partial \chi_1} \frac{\partial q}{\partial \chi_2} \right] dA \\ & + \int_A \left[ \sigma_{12}^{(2)} \frac{\partial z_1^{(1)}}{\partial \chi_1} \frac{\partial q}{\partial \chi_2} + \sigma_{22}^{(2)} \frac{\partial z_2^{(1)}}{\partial \chi_1} \frac{\partial q}{\partial \chi_2} - \sigma_{12}^{(2)} \frac{\partial z_1^{(1)}}{\partial \chi_2} \frac{\partial q}{\partial \chi_1} - \sigma_{22}^{(2)} \frac{\partial z_2^{(1)}}{\partial \chi_2} \frac{\partial q}{\partial \chi_1} \right] dA \end{aligned} \tag{A.5}$$

Using the stress-strain relation

$$I^{(1,2)} = \int_A h dA \quad \text{where } h = h_1 + h_2 + h_3 + h_4 + h_5 + h_6 - h_7 - h_8 \tag{A.6}$$

For plane stress

$$h_1 = \frac{E}{1-\nu^2} \left( \frac{\partial z_1^{(1)}}{\partial \chi_1} + \nu \frac{\partial z_2^{(1)}}{\partial \chi_2} \right) \frac{\partial z_1^{(2)}}{\partial \chi_1} \frac{\partial q}{\partial \chi_1} \tag{A.7-a}$$

$$h_2 = \frac{E}{2(1+\nu)} \left( \frac{\partial z_1^{(1)}}{\partial \chi_2} + \nu \frac{\partial z_2^{(1)}}{\partial \chi_1} \right) \frac{\partial z_1^{(2)}}{\partial \chi_1} \frac{\partial q}{\partial \chi_2} \tag{A.7-b}$$

$$h_3 = \frac{E}{2(1+\nu)} \left( \frac{\partial z_1^{(1)}}{\partial \chi_2} + \nu \frac{\partial z_2^{(1)}}{\partial \chi_1} \right) \frac{\partial z_2^{(2)}}{\partial \chi_1} \frac{\partial q}{\partial \chi_1} \tag{A.7-c}$$

$$h_4 = \frac{E}{1-\nu^2}\left(\nu\frac{\partial z_1^{(1)}}{\partial \chi_1} + \frac{\partial z_2^{(1)}}{\partial \chi_2}\right)\frac{\partial z_2^{(2)}}{\partial \chi_1}\frac{\partial q}{\partial \chi_2} \tag{A.7-d}$$

$$h_5 = \sigma_{12}^{(2)}\frac{\partial z_1^{(1)}}{\partial \chi_1}\frac{\partial q}{\partial x_2} \tag{A.7-e}$$

$$h_6 = \sigma_{22}^{(2)}\frac{\partial z_2^{(1)}}{\partial \chi_1}\frac{\partial q}{\partial x_2} \tag{A.7-f}$$

$$h_7 = \sigma_{12}^{(2)}\frac{\partial z_1^{(1)}}{\partial \chi_2}\frac{\partial q}{\partial x_1} \tag{A.7-g}$$

$$h_8 = \sigma_{22}^{(2)}\frac{\partial z_2^{(1)}}{\partial \chi_2}\frac{\partial q}{\partial x_1} \tag{A.7-h}$$

For plane strain,

$$h_1 = \frac{E}{(1+\nu)(1-2\nu)}\left[(1-\nu)\frac{\partial z_1^{(1)}}{\partial \chi_1} + \nu\frac{\partial z_2^{(1)}}{\partial \chi_2}\right]\frac{\partial z_1^{(2)}}{\partial \chi_1}\frac{\partial q}{\partial \chi_1} \tag{A.8-a}$$

$$h_2 = \frac{E}{2(1+\nu)}\left(\frac{\partial z_1^{(1)}}{\partial \chi_2} + \frac{\partial z_2^{(1)}}{\partial \chi_1}\right)\frac{\partial z_1^{(2)}}{\partial \chi_1}\frac{\partial q}{\partial \chi_1} \tag{A.8-b}$$

$$h_3 = \frac{E}{2(1+\nu)}\left(\frac{\partial z_1^{(1)}}{\partial \chi_2} + \frac{\partial z_2^{(1)}}{\partial \chi_1}\right)\frac{\partial z_2^{(2)}}{\partial \chi_1}\frac{\partial q}{\partial \chi_1} \tag{A.8-c}$$

$$h_4 = \frac{E}{(1+\nu)(1-2\nu)}\left[\nu\frac{\partial z_1^{(1)}}{\partial \chi_1} + (1-\nu)\frac{\partial z_2^{(1)}}{\partial \chi_2}\right]\frac{\partial z_2^{(2)}}{\partial \chi_1}\frac{\partial q}{\partial \chi_2} \tag{A.8-d}$$

$$h_5 = \sigma_{12}^{(2)}\frac{\partial z_1^{(1)}}{\partial \chi_1}\frac{\partial q}{\partial x_2} \tag{A.8-e}$$

$$h_6 = \sigma_{22}^{(2)}\frac{\partial z_2^{(1)}}{\partial \chi_1}\frac{\partial q}{\partial x_2} \tag{A.8-f}$$

$$h_7 = \sigma_{12}^{(2)}\frac{\partial z_1^{(1)}}{\partial \chi_2}\frac{\partial q}{\partial x_1} \tag{A.8-g}$$

$$h_8 = \sigma_{22}^{(2)}\frac{\partial z_2^{(1)}}{\partial \chi_2}\frac{\partial q}{\partial x_1} \tag{A.8-h}$$

# APPENDIX B

### Triangle-Rectangle mapping

The Gaussian points that obtained from the elements that arte cut by the crack after the partitioning are obtained using this function

```
function
[g_s,g_t,H,weight]=Triangle_rectangle_map(xcoord,ycoord,X1,X2,COEFF,ele_size)
%X1 : tip1 x-coordinate
%X2 : tip2 x-coordinate
%COEFF: the coefficients that represent the crack as y=COEFF(1)*X+COEFF(2)
%xcoord: the x-coordinates for the nodes of the bilinear element
%ycoord: the y-coordinates for the nodes of the bilinear element
%ele_size : the element edge length.
[Enriched_ELEMENT_INTERSEC]=Element_Crack_Intersection_points(xcoord,ycoord
,X1,X2,COEFF,ele_size);
  x_center= sum(xcoord)/4;
  y_center= sum(ycoord)/4;
  X1=Enriched_ELEMENT_INTERSEC(1);
  Y1=Enriched_ELEMENT_INTERSEC(2);
  X2=Enriched_ELEMENT_INTERSEC(3);
  Y2=Enriched_ELEMENT_INTERSEC(4);
  Area_Element=ele_size^2;
  negative_count=1;
  positive_count=1;
  for j=1:4
    x = xcoord(j);
    y = ycoord(j);
    delta = (X1-x)*(Y2-y)-(X2-x)*(Y1-y);
    if delta > 1e-6*ele_size
      H(j)=1;
    elseif delta < -1e-6*ele_size
      H(j)=-1;
    else
      H(j)=10;
    end
  end
  for j=1:4
    if H(j) == 1
      pos_vertex_x(positive_count)=xcoord(j);
      pos_vertex_y(positive_count)=ycoord(j);
      positive_count=positive_count+1;
    elseif H(j) == -1
```

```
        neg_vertex_x(negative_count)= xcoord(j);
        neg_vertex_y(negative_count)= ycoord(j);
        negative_count=negative_count+1;
    end
end
pos_vertex_x(positive_count)=Enriched_ELEMENT_INTERSEC(1);
pos_vertex_y(positive_count)=Enriched_ELEMENT_INTERSEC(2);
pos_vertex_x(positive_count+1)=Enriched_ELEMENT_INTERSEC(3);
pos_vertex_y(positive_count+1)=Enriched_ELEMENT_INTERSEC(4);
neg_vertex_x(negative_count)= Enriched_ELEMENT_INTERSEC(1);
neg_vertex_y(negative_count)= Enriched_ELEMENT_INTERSEC(2);
neg_vertex_x(negative_count+1)= Enriched_ELEMENT_INTERSEC(3);
neg_vertex_y(negative_count+1)= Enriched_ELEMENT_INTERSEC(4);
[pos_k,pos_Area] = convhull(pos_vertex_x,pos_vertex_y);
[neg_k,neg_Area] = convhull(neg_vertex_x,neg_vertex_y);
[max_val,I_inter_pos]=max(pos_k);
I_inter_pos=I_inter_pos-1;
[max_val,I_inter_neg]=max(neg_k);
%-------------------------------------------------------
x_pos_center= sum(pos_vertex_x)/length(pos_vertex_x) ;
y_pos_center= sum(pos_vertex_y)/length(pos_vertex_y) ;
x_neg_center= sum(neg_vertex_x)/length(neg_vertex_x);
y_neg_center= sum(neg_vertex_y)/length(neg_vertex_y);
for j=1:length(pos_vertex_x)
    sub_tri_pos(j,1)= pos_vertex_x(pos_k(j));
    sub_tri_pos(j,2)= pos_vertex_y(pos_k(j));
    sub_tri_pos(j,3)= pos_vertex_x(pos_k(j+1));
    sub_tri_pos(j,4)= pos_vertex_y(pos_k(j+1));
    sub_tri_pos(j,5)= x_pos_center;
    sub_tri_pos(j,6)= y_pos_center;
end
for j=1:length(neg_vertex_x)
    sub_tri_neg(j,1)= neg_vertex_x(neg_k(j));
    sub_tri_neg(j,2)= neg_vertex_y(neg_k(j));
    sub_tri_neg(j,3)= neg_vertex_x(neg_k(j+1));
    sub_tri_neg(j,4)= neg_vertex_y(neg_k(j+1));
    sub_tri_neg(j,5)= x_neg_center;
    sub_tri_neg(j,6)= y_neg_center;
end
for i=1:length(pos_vertex_x)
    x1=sub_tri_pos(i,1);
    y1=sub_tri_pos(i,2);
    x2=sub_tri_pos(i,3);
    y2=sub_tri_pos(i,4);
    x3=sub_tri_pos(i,5);
    y3=sub_tri_pos(i,6);
```

```
    child_weigth=2*abs(x1*y2+x2*y3+x3*y1-x1*y3-x2*y1-x3*y2)/Area_Element;
     a1=0.797426985353;b1=0.101286507323;a2=0.059715871789;
     b2=0.470142064105;w1=0.225;w2=0.125939180544;w3=0.132394152788;
     L1=[1/3 a1 b1 b1 a2 b2 b2];L2=[1/3 b1 a1 b1 b2 a2 b2];
     L3=[1/3 b1 b1 a1 b2 b2 a2];W=[w1 w2 w2 w2 w3 w3 w3];
    for j=1:length(W)
       N1=L1(j);
       N2=L2(j);
       N3=L3(j);
       x_glob(length(W)*(i-1)+j)= N1*x1+N2*x2+N3*x3;
       y_glob(length(W)*(i-1)+j)= N1*y1+N2*y2+N3*y3;
       weight(length(W)*(i-1)+j)=child_weigth*W(j);
       H(length(W)*(i-1)+j)=1;

    end
end
%--------------------------------------------------------------------------
base = length(x_glob);
for i=1:length(neg_vertex_x)
    x1=sub_tri_neg(i,1);
    y1=sub_tri_neg(i,2);
    x2=sub_tri_neg(i,3);
    y2=sub_tri_neg(i,4);
    x3=sub_tri_neg(i,5);
    y3=sub_tri_neg(i,6);
    child_weigth=2*abs(x1*y2+x2*y3+x3*y1-x1*y3-x2*y1-x3*y2)/Area_Element;
    a1=0.797426985353;b1=0.101286507323;a2=0.059715871789;
    b2=0.470142064105;w1=0.225;w2=0.125939180544;w3=0.132394152788;
    L1=[1/3 a1 b1 b1 a2 b2 b2];L2=[1/3 b1 a1 b1 b2 a2 b2];
    L3=[1/3 b1 b1 a1 b2 b2 a2];W=[w1 w2 w2 w2 w3 w3 w3];
    for j=1:length(W)
       N1=L1(j);
       N2=L2(j);
       N3=L3(j);
       x_glob(base+length(W)*(i-1)+j)= N1*x1+N2*x2+N3*x3;
       y_glob(base+length(W)*(i-1)+j)= N1*y1+N2*y2+N3*y3;
       weight(base+length(W)*(i-1)+j)=child_weigth*W(j);
       H(base+length(W)*(i-1)+j)=-1;
    end
end

for i=1:length(x_glob)
    g_s(i)=(x_glob(i)-x_center)*(2/ele_size);
    g_t(i)=(y_glob(i)-y_center)*(2/ele_size);
end
```

**Element degrees of freedom**

```
function [edof]=Element_dof(Node_type)
%Node_type is obtained from nodes_ID
edof=0;
for i=1:length(Node_type)
   if Node_type(i)==0
      edof = edof+2;
   elseif Node_type(i)==1 || Node_type(i)==-1 || Node_type(i)==10
      edof=edof+4;
   elseif Node_type(i)==11 || Node_type(i)==22
      edof=edof+10;
   end
end
```

**The extra degrees of freedom index**

```
Function [index_XFEM]=get_index(nodes_ID,sdof)
% sdof : is the regular system degrees of freedom
count=sdof;
index_XFEM (:,1)=0;
for i=1:length(nodes_ID)
  if nodes_ID(i)==1 || nodes_ID(i)==-1 || nodes_ID(i)==10
      index_XFEM (i)=count;
      count=count+2;
   elseif nodes_ID(i)==11 || nodes_ID(i)==22
      index_XFEM (i)=count;
      count=count+8;
   end
end
```